Enhancing NOMA Backscatter IoT Communications With RIS

Minh-Sang Van Nguyen[®], Dinh-Thuan Do[®], Senior Member, IEEE, Alireza Vahid[®], Senior Member, IEEE, Sami Muhaidat[®], Senior Member, IEEE, and Douglas Sicker, Senior Member, IEEE

Abstract—As potential solutions to empower transmissions among the Internet of Things (IoT) devices, ambient radio frequency (RF) backscatter technology and reconfigurable intelligent surfaces (RISs) have recently attracted a lot of attention. To improve energy and spectrum efficiency, we design a system with a transmit antenna selection (TAS)-aided base station (BS) relying on nonorthogonal multiple access (NOMA), RIS, and backscatter communications (BackCom) with robust transmission links, allowing more users to be served effectively. We adopt the twouser grouping model in the coverage of main BS associated with a particular RIS and interference from coordinate BS is also considered to showcase differences among the performance of the two different kinds of users (i.e., the IoT user with and the IoT user without a dedicated RIS). To exhibit the system performance, we derive closed-form expressions for two main system performance metrics, namely, outage probability and ergodic capacity. A degraded performance is also considered for the case of imperfect successive interference cancellation (SIC). The benefits of the BackCom RIS-aided NOMA system are then demonstrated by comparing its performance to that of traditional orthogonal multiple access (OMA) RIS-aided backscatter systems. We then introduce analytical models to characterize the impact of the main factors on the outage performance and characterize the optimal performance in specific cases. Together with extensive simulations, our analysis shows that the system performance can be adjusted by controlling factors, including power allocation coefficients, the number of metasurfaces of RIS, and target rates.

Manuscript received 12 June 2023; accepted 11 August 2023. Date of publication 25 August 2023; date of current version 6 February 2024. The work of Alireza Vahid was supported in part by the National Science Foundation (NSF) under Grant ECCS-2030285, Grant CNS-2106692, and Grant CNS-2211804. (Corresponding author: Alireza Vahid.)

Minh-Sang Van. Nguyen is with the Data Science Laboratory, Faculty of Information Technology, Ton Duc Thang University, Ho Chi Minh City 70000, Vietnam (e-mail: nguyenvanminhsang@tdtu.edu.vn).

Dinh-Thuan Do is with the School of Engineering, University of Mount Union, Alliance, OH 44601 USA (e-mail: doth@mountunion.edu).

Alireza Vahid is with the Department of Electrical and Microelectronic Engineering, Rochester Institute of Technology, Rochester, NY 14623 USA (e-mail: arveme@rit.edu).

Sami Muhaidat is with the Department of Electrical Engineering and Computer Science, Center for Cyber-Physical Systems, Khalifa University, Abu Dhabi, UAE (e-mail: muhaidat@ieee.org).

Douglas Sicker is with the Department of Computer Science and Engineering and the Department of Electrical Engineering, University of Colorado at Denver, Denver, CO 80204 USA (e-mail: douglas.sicker@ucdenver.edu).

Digital Object Identifier 10.1109/JIOT.2023.3308786

Index Terms—Backscatter, ergodic capacity, Internet of Things (IoT), reconfigurable intelligent surfaces (RISs), symbiotic radio (SR).

I. Introduction

UE TO improvements in spectrum efficiency and user fairness, nonorthogonal multiple access (NOMA) has been proposed as an effective approach to accommodate the high data traffic in the Internet of Things (IoT) networks [1], [2], [3], [4], [5], [6]. The conventional orthogonal multiple access (OMA) allows only one user to access the networks in each orthogonal resource block (e.g., a time slot, a frequency channel, a spreading code, or an orthogonal spatial degree of freedom), which results in wasted resources. In contrast, NOMA allows more than one user to access the network in the same resource block. The beyond 5G (B5G)-enabled massive IoT systems deal with massive connectivity and limited energy situations that could be crucial challenges to maintain diversified Qualify of Service (QoS) of a large number of IoT devices. An overlay cognitive NOMA system has been explored in [1] to evaluate the performance of a primary transmitter-receiver pair. In such IoT applications, an energy harvesting (EH)based secondary transmitter (ST) adopts a time-switching (TS)/power-splitting (PS) architecture to harvest the energy from the primary transmission through the radio frequency (RF) signals. Liu et al. [4] developed multiuser detection in uplink IoT systems by enabling NOMA and successive interference canceler (SIC)-based detectors. They emphasized the performance of reliable transmission guaranteed by a joint maximum-likelihood (JML) detector. To gain the main benefit of the proposed model, a closed-form upper bound of bit error rate (BER) was derived over Rayleigh fading channels in which an adaptive M-ary phase shift keying (M-PSK) is adopted. Do et al. [3] studied the industrial IoT over cognitive heterogeneous NOMA networks by considering the scheduling and power allocation problems for an uplink from the secondary IoT devices under two undesirable situations including imperfect spectrum sensing and imperfect channel state information (CSI). The network throughput constrained by the total power at each secondary IoT device could be maximized by relying on joint secondary IoT device scheduling and power allocation approaches. The main results focus on the evaluation of the tradeoff among the system performance and the number of secondary IoT devices, the fairness transmission rate among different secondary IoT devices, and the interference power threshold at each primary source.

2327-4662 © 2023 IEEE. Personal use is permitted, but republication/redistribution requires IEEE permission. See https://www.ieee.org/publications/rights/index.html for more information.

A. Backscatter Communications

Recently, backscatter communications (BackCom) with the capability of passive RF identification (RFID) has emerged as a promising paradigm to deploy IoT systems [7]. In principle, a reader transmits a portion of the RF signals to reflect and modulate for information transmission, while energy is converted from the remaining portion for circuit operation. Deng et al. [8] introduced tag selection in backscatter networks as a great approach to enhance the system outage performance. To enhance the spectrum and energy efficiency (EE), Elsayed et al. [9] studied backscatter networks with improved performance for battery-limited devices. Ma et al. [10] presented a model of the aggregate interference from the sporadic backscatter transmissions. They derived expressions of the covert outage probability and the transmission success probability to highlight the reliability of backscatter systems. The work in [11] considered a cognitive ambient backscatter system to deploy the green IoT. In this scenario, by simultaneously sharing both spectrum and RF sources, backscatter device (BD) support to obtain better outage performance. By jointly using the power beacons (PB)'s beamforming for a BackCom network and optimizing the relay strategy and a PB-based EH, the system capacity can be maximized [12]. Ye et al. [13] presented the optimal EE by jointly optimizing the PB's transmit time, the PB's transmit power, and the reflection coefficient for the EH-based BackCom system.

Since NOMA benefits to BackCom, Li et al. [14] explored three benchmark systems including the NOMA relaying scheme, the NOMA scheme without relay, and the incremental relaying NOMA scheme. In particular, they analyzed the expected rate, the outage performance, and the diversitymultiplexing tradeoff performance. To achieve optimal secrecy rate, Khan et al. [15] investigated an optimization problem for a multicell backscatter system relying on NOMA in the presence of multiple eavesdroppers. In particular, the reflection coefficients can be optimized for the backscatter node. They formulated the optimization problem as a convex problem. A similar work in [16] implemented a protocol integrating dynamic time-division multiple access with NOMA to examine the performance of a NOMA bistatic BackCom network where a backscatter receiver is operated with the help of multiple BDs. By jointly optimizing power reflection coefficients and the BDs' backscatter time, the minimum throughput can be maximized among all BDs under some constraints including the BDs' harvested energy.

B. Reconfigurable Intelligent Surfaces

In recent studies [17], [18], by smartly reflecting signals toward the receiver in the cellular networks, reconfigurable intelligent surface (RIS)-aided systems have attracted a lot of attention due to their capability of extending cell coverage. Zhu et al. [17] presented an RIS-aided NOMA (RIS-NOMA) system by enabling extra information bits to be transmitted with proper subsurfaces to different users. They proved via closed-form expression on BER the improvement of the spectral efficiency. Gao et al. [19] studied an RIS-NOMA

system in two scenarios, i.e., beamformer-based NOMA and cluster-based NOMA schemes when the multiantenna base station (BS) is deployed. By considering massive multiple-input—multiple-output (MIMO), Zhi et al. [18] explored the performance of uplink RIS-aided networks in the presence of direct links. They designed the phase shifts of the RIS based on the statistical CSI. In particular, the closed-form expressions were derived in terms of the ergodic data rate. To solve the sum data rate maximization problem, they deployed a genetic algorithm (GA) based on the derived formula.

C. Related Works

Li et al. [20] studied a downlink RIS-aid BackCom relying on advanced features of NOMA in which the wireless channels with Rayleigh distribution are assumed. They focused on the scenario of two-user in a cluster with channel disparity from the BS. The main finding in that work is deriving outage probability expressions. They confirmed reflection coefficients and the number of reflecting RIS elements can be configured separately to showcase differences in user performance. The optimal power allocation for the two users was not studied. In contrast to [20], the recent work in [21] solved the problem of how to improve the network performance by achieving two optimal parameters of BackCom RIS-NOMA networks, i.e., the phase shifts and the power resource allocation. Their results deal with how to assist the cell-edge user (CEU) to communicate with the BS while retaining the performance improvement in terms of the EE and the sum rate. To further evaluate the sum rate of BackCom RIS-NOMA, the work in [22] considered the simple scenario of a single-antenna BS leveraging NOMA and an M-passive reflecting elements RIS to better serve two single-antenna users (strong user and weak user). They developed an alternating optimization (AO) algorithm to obtain the optimal sum rate of strong user by optimizing the RIS phase shifts and power splitting coefficients at the BS while guaranteeing the QoS for weak user.

D. Motivation and Contributions

The system models in [20], [21], and [22] studied networks with single-antenna users throughout the network, which limits the performance of IoT devices. Further, Chen et al. [23] explored the advantages of the RIS in a symbiotic radio (SR) system. The authors jointly designed the passive beamforming of the RIS and the active transmit beamforming of the BS to minimize the BS's transmission power with two constraints including the rate constraint for the primary communication and the signal-to-interference-plus-noise ratio (SINR) for decoding the backscatter signals. To explore the BackCom system, Hu et al. [24] presented a novel RIS-enhanced downlink multiuser multi-input-single-output (MU-MISO) scheme. In the proposed system, each RIS acts as an IoT device to enable IoT transmissions to the same primary receiver and improve the primary transmission from the primary transmitter to the corresponding primary receiver nearby. However, the performance improvement for CEUs in the NOMA scheme is still necessary to study more. Although two BSs can work together to improve the performance of CEUs as reported

	Our Scheme	[27]	[28]	[29]	[30]	[31]
BackCom OMA / BackCom SR	X	х	Х	х	х	х
NOMA BackCom	x	х				
TAS	x					
Interference from nearby BS	x					
Multi-RIS	x				X	
RIS with random phase-shift	x					
The imperfect SIC	x					
Interference from nearby devices	x					
Diversity order	x					
Outage probability/BER	x			X		x
Ergodic capacity	X					
System throughput	X					
Asymptotic analysis	X					

TABLE I
COMPARISON OF THIS ARTICLE WITH SIMILAR STUDIES

in [25], but how the system deals with the worse case that CEUs cannot connect with nearby BS.

These results motivate us to study an effective framework for BackCom IoT systems. In particular, our work takes into account the advantages of the RIS and focuses on investigating the performance of CEUs in BackCom RIS-NOMA systems. To leverage higher diversity order of multiple-antenna structures, we consider the more sophisticated case of BackCom IoT system when transmit antenna selection (TAS) is adopted at the BS [26]. We also evaluate the impact of interference from the nearby BS to CE and cell-center IoT devices locating in a cluster¹ and compare their performance with two benchmarks.

A comparison of our work with other related papers is also presented in Table I. Our main contributions are as follows.

- 1) We propose a new system model with multiple users assigned to multiple clusters. We just evaluate the degraded performance of cell-center and CEUs situated in a specific cluster associated with the links from the RIS and BD while experiencing interference from a nearby BS. The CCU, which is close to the BS, just needs the help of BS to improve its performance; while the CEU requires the RIS to enhance its performance. By adopting a fixed power allocation scheme to the two users, we show the performance of these two devices improves significantly thanks to the RIS, the TAS, and NOMA techniques.
- 2) We derive an expression to achieve explicit system performance analysis, i.e., the outage probability and ergodic capacity for the BD and the cell-center and CEUs by comparing the main proposed BackCom NOMA-RIS with two benchmarks, namely, traditional NOMA BackCom [32] and BackCom OMA-RIS systems.

¹Two BSs are arranged to provide relevant coverage. However, the CEUs may experience high levels of interference from the nearby BS if the CEU cannot work with the cell-center user (CCU) to create a pair associated with these BSs. It is noted that two BSs in this circumstance work to form coordinated multipoint transmission (CoMP) [25]. In doing so, at least two BSs coordinate to serve the users simultaneously. In practice, some CEUs fail to connect with the relevant BS and cannot find a way to pair with CCUs. Thus, the CEUs located in particular clusters in our model are considered as failed CEUs in joint-transmission CoMP NOMA-based systems. In this case, CEUs still experience a strong intercell interference from the adjacent BS.

3) To provide further insights in BackCom systems, we provide the asymptotic analyses and diversity order for the outage performance of BackCom NOMA-RIS. The expected performance is illustrated via simulations to conclude that the number of transmit antennas, the number of metasurface elements at the RIS, the power allocation factors, and the target rates are the main parameters in deciding the performance of the IoT devices.

E. Organization and Notations

The remainder of this article is organized as follows. Section II provides the system model of user relaying in the downlink NOMA BackCom system relying on RIS and BackCom techniques. Section III presents the analytical expressions for outage probability performance. Section IV presents the ergodic capacity performance of the BackCom NOMA-RIS system. Numerical results are presented in Section V to demonstrate the outage performance of the proposed schemes. Finally, Section VI concludes this article.

The main notations of this article are as follows: $\Pr(\cdot)$ denotes the probability operator; $E[\cdot]$ denotes the expectation operator; $f_X(\cdot)$ and $F_X(\cdot)$ denote the probability distribution function (PDF) and the cumulative distribution function (CDF), respectively; $CN(\cdot,\cdot)$ is a circularly symmetric complex Gaussian distribution; \sim stands for "distributed as"; $|\cdot|$ is an absolute operator; and $Ei(\cdot)$ denotes the exponential integral function [33, eq. (8.211.1)]. An identity matrix of size $M \times M$ is denoted by I_M ; $(\cdot)^H$ denotes the conjugate and Hermitian transpose; and a diagonal matrix with s_1, \ldots, s_M on the diagonal is denoted by $\operatorname{diag}(s_1, \ldots, s_M)$.

II. SYSTEM MODEL

We consider a downlink NOMA BackCom IoT system with two BSs enhanced by RIS and TAS techniques as shown in Fig. 1. An RIS is composed of M reflecting elements. The backscatter device (denoted by BD) is required to serve both CCU D_1 and CEU D_2 , which are affected by the interference from a nearby BS (BS_2). All devices in the context of this BackCom NOMA-RIS are usually designed to have a single antenna except for the BS, which is equipped with multiple antennas. Having a single-antenna BD and cell-edge and

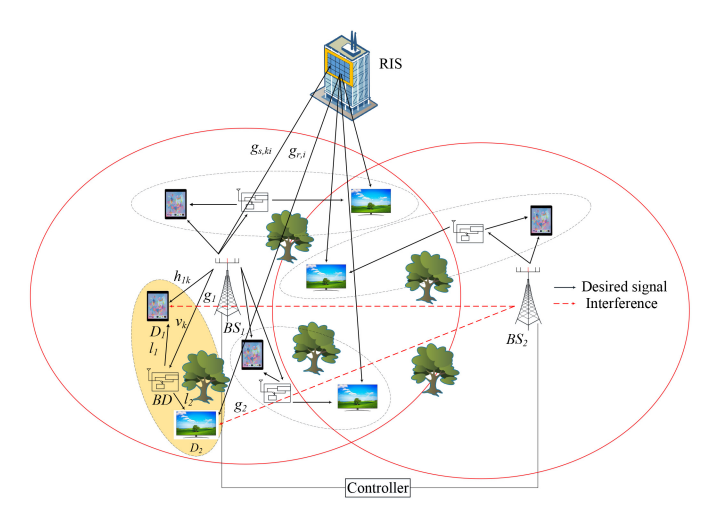


Fig. 1. System model for BackCom NOMA-RIS IoT.

TABLE II KEY PARAMETERS

Symbol	Description
x_n	The messages with unit power transmitted to D_n with
	(n=1,2)
s	The BD backscatters the BS_1 's signal to D_n
x_{dn}	The interference symbol from BS_2 to D_n
θ	A complex reflection coefficient used to normalize s
β_n	The power allocation parameters for x_n with $0 < \beta_n < 1$
P	The total transmit power of the BS_1
P_{dn}	The transmit power from BS_2 to D_n
τ	The RIS attenuation factor
R_n	The target rate for D_n
R_s	The target rate for BD
σ_n	The complex Gaussian noise at D_n with $\sigma_n \sim CN(0, N_0)$
$g_{s,ki}$	The channels from the BS_1 to RIS
$g_{r,i}$	The channels from the RIS to user D_2
h_{1k}	The channel response from the BS_1 to the first user D_1
v_k	The channel response from the the BS_1 to BD
l_n	The channel response from the BD to D_n
g_n	The channel response from BS_2 to D_n

cell-center IoT users are expected to avoid excessive power requirements and complex detection circuitry, thereby leveraging the benefits of the BackCom technique. The CCU D_1 has a direct link to the BS_1 , while the CEU D_2 needs the assistance of the RIS to improve its performance. To characterize wireless links, let $h_{1k} \sim CN(0, \varphi_1)$, $v_k \sim CN(0, \varphi_v)$, $l_1 \sim CN(0, \varphi_{l,1})$, $l_2 \sim CN(0, \varphi_{l,2})$, $g_1 \sim CN(0, \varphi_{g,1})$, and $g_2 \sim CN(0, \varphi_{g,2})$. In what follows, we provide the received signal and SINR models at D_1 and D_2 . The main parameters can be found in Table II.

A. Received Signals at D_1

Following the NOMA principle, multiple signals are processed at the BS_1 , and their superposition would be the

transmit signal given by

$$x = \sqrt{\beta_1} x_1 + \sqrt{\beta_2} x_2. \tag{1}$$

It is assumed that $\beta_2 > \beta_1$ and $\beta_1 + \beta_2 = 1$ due to the different service requirements of the two devices.³ Considering the power-domain NOMA technique, NOMA users can be distinguished by dividing the power levels. It is noted that if one of the NOMA users is far from the BS, its performance can be enhanced by having a higher transmit power. Such power allocation scheme applied to the weak and strong users is designed following the principle of decoding order in NOMA-aided systems. In particular, the decoding order of paired users (the weak and strong users) severely relies on their channel qualities.

To enable BackCom functionality, BD backscatters the BS_1 's signal to D_1 with its own message s, where $E[|s|^2] = 1$. There are two types of signals processed at D_1 : direct link signal from the BS_1 and the backscatter link signal from the BD. In particular, the received signals at D_1 can be given as [32], [35], [36]

$$y_{1} = \frac{\sqrt{P}h_{1k}}{\sqrt{d_{h_{1}}^{\partial}}}x + \sqrt{P_{d_{1}}}g_{1}x_{d_{1}} + \frac{\theta\sqrt{P}v_{k}l_{1}}{\sqrt{(d_{v} + d_{l_{1}})^{\partial}}}xs + \sigma_{1}$$

$$= \frac{\sqrt{P}h_{1k}}{\sqrt{d_{h_{1}}^{\partial}}}\sqrt{\beta_{1}}x_{1} + \frac{\sqrt{P}h_{1k}}{\sqrt{d_{h_{1}}^{\partial}}}\sqrt{\beta_{2}}x_{2}$$

$$= \frac{\sqrt{P}h_{1k}}{\sqrt{d_{h_{1}}^{\partial}}}\sqrt{d_{h_{1}}^{\partial}}\sqrt{d_{h_{1}}^{\partial}}\sqrt{d_{h_{1}}^{\partial}}\sqrt{d_{h_{1}}^{\partial}}\sqrt{d_{h_{1}}^{\partial}}\sqrt{d_{h_{1}}^{\partial}}\sqrt{d_{h_{1}}^{\partial}}\sqrt{d_{h_{1}}^{\partial}}\sqrt{d_{h_{1}}^{\partial}}\sqrt{d_{h_{1}}^{\partial}}\sqrt{d_{h_{1}}^{\partial}}\sqrt{d_{h_{1}}^{\partial}}\sqrt{d_{h_{1}}^{\partial}}\sqrt{d_{h_{1}}^{\partial}}\sqrt{d_{h_{1}}^{\partial}}\sqrt{d_{h_{$$

where d_{h_1} , d_{ν} , and d_{l_1} denote the distances from BS_1 to D_1 , from BS_1 to BD, and from BD to D_1 , respectively. We also denote by ∂ as the large-scale path-loss factor for all the links. It is generally considered that backscatter has sum-distance path loss, while RIS has product-distance path loss [37], [38]. By reconsidering (2), when the superimposed signal containing x_1 and x_2 transmitted from BS_1 to user D_1 , which also receives signal from BD and interference from BS_2 , the quality of received signal at D_1 becomes worse. It is worth noting that D_1 wishes only to decode its own signal, x_1 (the first component is considered as the expected signal, while x_2 in the second component stands for intracluster interference, and x_{d1} in the third component represents as interference from BS_2 [36]).

The signal decoding order at each receiver follows the corresponding signal power level starting with the signal having the highest allocated power, i.e., x_2 , x_1 and then s (the signal from the BD, s, has very low power and thus, is typically received with the lowest power and decoded last) [32], [39].

²This model can be considered a compact model applied in IoT compared to the work in [34]. The practical models using nine BSs and a total of 36 transmitter–receiver radio links were deployed via the measurement campaign [34]. These BSs can be operated together for improving the performance of urban micro-cell where leverages a large-scale mmWave BS diversity measurement at 73 GHz (conducted at downtown, Brooklyn, NY, USA).

³In downlink IoT systems, when the BS provides dynamic services to different NOMA devices, it benefits by deploying both NOMA and BackCom techniques to improve performance at devices. We consider the framework of a two-user group [20], [21]. We should not examine multiple users in a cluster since we expect to indicate the maximum advances of RIS-NOMA BackCom with respect to performance improvement at different IoT devices, which exhibit less impairment originated by interference from intracluster devices.

The first user, D_1 , starts by decoding x_2 , then x_1 , and finally s with the SIC technique. The SINR for decoding x_2 is given by

$$\gamma_{1k\leftarrow2} = \frac{\beta_2 P d_{h_1}^{-\partial} |h_{1k}|^2}{\beta_1 P d_{h_1}^{-\partial} |h_{1k}|^2 + P \wp_1 |v_k|^2 |l_1|^2 + P_{d1} |g_1|^2 + N_0}$$
(3)

where $\wp_1 = |\theta|^2 (d_v + d_{l_1})^{-\partial}$.

By assuming that x_2 can be decoded successfully, it can be subtracted from y_1 and then D_1 decodes its own message x_1 . Therefore, by doing this, the SINR is given by

$$\gamma_{1k} = \frac{\beta_1 P d_{h_1}^{-\partial} |h_{1k}|^2}{P_{\S^2 1} |v_k|^2 |l_1|^2 + P_{d_1} |g_1|^2 + N_0}.$$
 (4)

Further, assuming x_1 is perfectly decoded, the BD's message s can then be decoded at D_1 . Given x, the SINR to decode s at D_1 can be formulated by [32], $[39]^4$

$$\gamma_{sk} = \frac{P\wp_1|v_k|^2|l_1|^2}{P_{d1}|g_1|^2 + N_0}. (5)$$

B. Received Signals at D2

Similar to [36], the received signals at D_2 can be written as (6), shown at the bottom of the page. We denote the distances from the BS_1 to the RIS, from the RIS to D_2 , and from the BD to D_2 by d_{sr} , d_{rd_2} , and d_{l_2} , respectively [37], [38]. Similar to the explanation of (2), in (6), the first component x_2 is considered as the expected signal, while x_1 in the second component stands for intracluster interference, and x_{d2} in the third component represents as interference from BS_2 [36]. By treating other signal components as interference, D_2 only decodes its own message D_2 . To decode signal D_2 , the corresponding SINR is formulated by [38]

$$\gamma_{2k} = \frac{\beta_2 \tau P d_{sr}^{-\partial} d_{rd_2}^{-\partial} Q_{1k}^2}{\beta_1 \tau P d_{sr}^{-\partial} d_{rd_2}^{-\partial} Q_{1k}^2 + P_{\wp_2} |v_k|^2 |l_2|^2 + P_{d2} |g_2|^2 + N_0}.$$
(7)

In order to simplify the analysis, ideal passive beamforming (IPB) with perfect channel estimation (PCE) is assumed at the RIS [40], and all elements have the same reflection amplitude. We have the phase $\varpi_i = -\arg(g_{s,ki}g_{r,i})$ [40]. $\wp_2 = -\arg(g_{s,ki}g_{r,i})$

 4 It is worth pointing out that the normal BackCom NOMA system turns into a BackCom system if the source BS does not serve D_2 . In this case, β_1 is equal to 1, i.e., $x = \sqrt{P}x_1$. The received signal at D_1 in the BackCom system is expressed as (2). In BackCom SR, D_1 first decodes x_1 then s and the corresponding SINR and SNR are given by (4) and (5) with $x_1 = 1$, respectively. Further, if BD does not exist, the conventional downlink NOMA system could be considered.

 $|\theta|^2 (d_v + d_{l_2})^{-\partial}$, due to $\sum_{i=1}^M g_{s,ki} g_{r,i} e^{i\overline{\omega}_i} = \sum_{i=1}^M |g_{s,ki}| |g_{r,i}|$ in the case of perfect CSI. We need to define a new variable $Q_{1k} \triangleq \sum_{i=1}^M |g_{s,ki}| |g_{r,i}|$. To further analyze system performance (outage probability), Q_{1k} can be approximated with an exponential random variable with parameter $Q_{1k} \sim \text{Exp}(M)$ [38].

The base station, BS_1 , will select the best channel to transmit the signal to user D_1 , the BD, and RIS, out of its available K antennas. For the best link from BS_1 to D_1 , BS_1 to BD, and BS_1 to RIS, the best antenna of BS_1 can be selected by the following criterion $k^* = \arg \max_{k} (X_k)$ [41], where $X_k \in$

$$\{|h_{1k}|^2, |\widetilde{h}_{1k}|^2, Q_{1k}^2, Z_k^2, |v_k|^2\}.$$

In the following section, we will analyze the outage probability as the main system performance metric to better understand the BackCom RIS-NOMA system. The performance of the conventional BackCom NOMA without RIS was reported in [42] and thus, we will not recall it here.

III. OUTAGE PERFORMANCE ANALYSIS

As an important system performance metric, the outage probability needs to be evaluated when the target rates of the users are determined by their required QoS. We will study the outage probability performance under three scenarios including the BackCom RIS-NOMA and the (two) benchmark BackCom systems described in the next section.

A. Outage Probability of D_1

With regard to the NOMA protocol, if D_1 fails to decode x_1 , it means that this event as an outage event. We assume to conduct perfect SIC in this case. To successfully decode x_1 , two conditions need to be met: 1) D_1 can decode x_2 successfully and 2) D_1 can decode its own information x_1 successfully. Then, the outage probability at D_1 can be written as [32], [35]

$$OP_1 = 1 - \underbrace{\Pr(\gamma_{1k^* \leftarrow 2} \ge \gamma_{\text{th2}}, \gamma_{1k^*} \ge \gamma_{\text{th1}})}_{\Delta}$$
(8)

where $\gamma_{thn} = 2^{R_n} - 1$.

Proposition 1: The closed-form expression for the outage probability at D_1 is given by

$$OP_{1} = 1 + \sum_{a=1}^{K} \sum_{b=1}^{K} {K \choose a} {K \choose b} (-1)^{a+b-2} \frac{\varphi_{1} \chi_{1}}{a \Omega_{1} P_{d1} \varphi_{g,1} + \varphi_{1}} \times e^{\chi_{1} - \frac{a \Omega_{1} N_{0}}{\varphi_{1}}} \operatorname{Ei}(-\chi_{1})$$
(9)

$$y_{2} = \sum_{i=1}^{M} \frac{\tau g_{s,ki} g_{r,i} e^{j\varpi_{i}}}{\sqrt{d_{sr}^{\partial} d_{rd_{2}}^{\partial}}} x + \frac{\theta v_{k} l_{2}}{\sqrt{\left(d_{v} + d_{l_{2}}\right)^{\partial}}} x s + \sqrt{P_{d2}} g_{2} x_{d2} + \sigma_{2}$$

$$= \sum_{i=1}^{M} \frac{\tau g_{s,ki} g_{r,i} e^{j\varpi_{i}}}{\sqrt{d_{sr}^{\partial} d_{rd_{2}}^{\partial}}} \sqrt{P\beta_{2}} x_{2} + \sum_{i=1}^{M} \frac{\tau g_{s,ki} g_{r,i} e^{j\varpi_{i}}}{\sqrt{d_{sr}^{\partial} d_{rd_{2}}^{\partial}}} \sqrt{P\beta_{1}} x_{1} + \underbrace{\sqrt{P_{d2}} g_{2} x_{d2}}_{\text{interference from } BS_{2}} + \frac{\theta v_{k} l_{2}}{\sqrt{\left(d_{v} + d_{l_{2}}\right)^{\partial}}} x s + \sigma_{2}. \tag{6}$$

where $\Omega_1 = \max((\gamma_{\text{th}2}/[(\beta_2 - \gamma_{\text{th}2}\beta_1)Pd_{h_1}^{-\partial}]), (\gamma_{\text{th}1}/[\beta_1Pd_{h_1}^{-\partial}]))$ and $\chi_1 = (b\varphi_1/[a\Omega_1P\wp_1\varphi_v\varphi_{l,1}]).$

Proof: The details are given in Appendix A.

B. Outage Probability of BD

By assuming perfectly decoding x_2 and x_1 , the BD's message can be successfully decoded properly. Thus, the outage probability of BD is given by [32], [35]

$$OP_{\mathrm{BD}} = 1 - \underbrace{\Pr(\gamma_{1k^* \leftarrow 2} \ge \gamma_{\mathrm{th}2}, \gamma_{1k^*} \ge \gamma_{\mathrm{th}1}, \gamma_{sk^*} \ge \gamma_{thb})}_{\Theta}$$

$$(10)$$

where $\gamma_{thb} = 2^{R_s} - 1$.

Proposition 2: The exact expression of the outage probability at device BD is given by

$$OP_{BD} = 1 - \sum_{a=1}^{K} \sum_{b=1}^{K} {K \choose a} {K \choose b} (-1)^{a+b-2} \times \frac{b\varphi_1}{\varphi_{g,1} \chi_3 (a\Omega_1 P \wp_1 \varphi_v \varphi_{l,1} + b\varphi_1)} e^{-\frac{\chi_2 \gamma_{lhb} N_0}{P_{\wp_1}} - \frac{a\Omega_1 N_0}{\varphi_1}}$$
(11)

where $\chi_2 = ([a\Omega_1 P_{\wp_1}]/\varphi_1) + (b/[\varphi_\nu \varphi_{l,1}])$ and $\chi_3 = ([\chi_2 \gamma_{\text{th}b} P_{d1}]/P_{\wp_1}) + ([a\Omega_1 P_{d1}]/\varphi_1) + (1/\varphi_{g,1}).$

Proof: The details are given in Appendix B.

C. Imperfect SIC Case for D₁

Considering imperfect SIC circumstance, the SINR of D_1 is formulated by [43]

$$\gamma_{1k^*,ip} = \frac{\beta_1 P d_{h_1}^{-\partial} |h_{1k^*}|^2}{\beta_2 P d_{h_1}^{-\partial} |\widetilde{h}_{1k^*}|^2 + P_{\mathcal{O}_1} |v_{k^*}|^2 |l_1|^2 + P_{d_1} |g_1|^2 + N_0}$$
(12)

where $|\widetilde{h}_{1k}|^2 \sim CN(0, k_1\varphi_{ip})$, the level of residual interference associated with SIC imperfection at D_1 is denoted by k_1 with $0 \le k_1 \le 1$ [43]. It is noted that $k_1 = 0$ and $k_1 = 1$ represent perfect SIC and no SIC, respectively.

The outage probability of D_1 corresponding imperfect SIC case is expressed by

$$OP_{1,ip} = 1 - \Pr(\gamma_{1k^* \leftarrow 2} \ge \gamma_{\text{th}2}, \gamma_{1k^*,ip} \ge \gamma_{\text{th}1}).$$
 (13)

Proposition 3: The closed-form expression for the outage probability at D_1 for imperfect SIC can be obtained as (14), shown at the bottom of the page, $\chi_4 = ([c\beta_1 d_{h_1}^{-\partial} \varphi_1]/[a\gamma_{\text{th}1} \wp_1 \varphi_\nu \varphi_{l,1}])$, $\chi_5 = ([(\beta_2 - \gamma_{\text{th}2} \beta_1) b d_{h_1}^{-\partial} \varphi_1]/[a\gamma_{\text{th}2} \wp_1 \varphi_\nu \varphi_{l,1}])$, $u_1 = ([\gamma_{\text{th}1} \beta_2]/[\gamma_{\text{th}2} + \gamma_{\text{th}1} \gamma_{\text{th}2}])$, and $u_2 = (\beta_2/\gamma_{\text{th}2})$.

Proof: The details are given in Appendix C.

Remark 1: From result in (14), the outage behavior can be determined by several parameters, such as the number of transmit antennas, K, the transmit SNR at the BS, and power allocation factors following NOMA β_1 , β_2 and target rates $\gamma_{\text{th}1}$, $\gamma_{\text{th}2}$. However, the transmit SNR at the BS still plays an important role to provide good performance at users.

D. Outage Probability of D₂

According to the NOMA protocol, the outage events of D_2 occur when D_2 cannot decode message x_2 successfully. Different from the performance of user D_1 , user D_2 can achieve significant improvement by enabling the RIS. The outage probability of D_2 is expressed as [32], [35]

$$OP_2 = 1 - \underbrace{\Pr(\gamma_{2k^*} \ge \gamma_{\text{th}2})}_{\Psi}. \tag{15}$$

Proposition 4: The closed-form expression for the outage probability at D_2 is given by

$$OP_{2} = 1 + \sum_{a=1}^{K} \sum_{b=1}^{K} {K \choose a} {K \choose b} (-1)^{a+b-2}$$

$$\times \frac{\chi_{6}(\beta_{2} - \gamma_{\text{th}2}\beta_{1})\tau PMd_{sr}^{-\partial} d_{rd_{2}}^{-\partial}}{a\gamma_{\text{th}2}P_{d2}\varphi_{g,2} + (\beta_{2} - \gamma_{\text{th}2}\beta_{1})\tau PMd_{sr}^{-\partial} d_{rd_{2}}^{-\partial}}$$

$$\times e^{\frac{\alpha\gamma_{\text{th}2}N_{0}}{(\beta_{2} - \gamma_{\text{th}2}\beta_{1})\tau PMd_{sr}^{-\partial} d_{rd_{2}}^{-\partial}}}$$

$$\times e^{(16)}$$

where $\gamma_{\text{th}2} = 2^{R_2} - 1$ and $\chi_6 = ([(\beta_2 - \gamma_{\text{th}2}\beta_1)b\tau Md_{sr}^{-\partial}d_{rd}^{-\partial}]/[a\gamma_{\text{th}2}\beta_2\varphi_\nu\varphi_{l,2}])$.

Proof: Based on (15), Ψ can achieve the result as shown in (17), at the bottom of the next page.

By referring to [33, eq. (3.352.4)] and applying some polynomial expansion manipulations, Ψ is further computed by

$$\Psi = -\sum_{a=1}^{K} \sum_{b=1}^{K} {K \choose a} {K \choose b} (-1)^{a+b-2}$$

$$\times \frac{\chi_{6}(\beta_{2} - \gamma_{\text{th}2}\beta_{1}) \tau PM d_{sr}^{-\partial} d_{rd_{2}}^{-\partial}}{a \gamma_{\text{th}2} P_{d2} \varphi_{g,2} + (\beta_{2} - \gamma_{\text{th}2}\beta_{1}) \tau PM d_{sr}^{-\partial} d_{rd_{2}}^{-\partial}}$$

$$\times e^{\chi_{6} - \frac{a \gamma_{\text{th}2} N_{0}}{(\beta_{2} - \gamma_{\text{th}2}\beta_{1}) \tau PM d_{sr}^{-\partial} d_{rd_{2}}^{-\partial}} \text{Ei}(-\chi_{6}).$$
(18)

By substituting (18) into (15), we can obtain (16). The proof is completed.

Remark 2: From result in (16), the outage behavior depends on many parameters as mentioned in the previous remark, but the number of reflecting elements in RIS still contributes to performance improvement at the users.

$$OP_{1,ip} = \begin{cases} 1 + \sum_{a=1}^{K} \sum_{b=1}^{K} \sum_{c=1}^{K} {K \choose a} {K \choose b} {K \choose c} (-1)^{a+b+c-3} \frac{b\beta_{1}\varphi_{1}}{a\gamma_{\text{th}1}\beta_{2}k_{1}\varphi_{ip} + b\beta_{1}\varphi_{1}} \frac{\beta_{1}Pd_{h_{1}}^{-\partial}\varphi_{1}\chi_{4}}{a\gamma_{\text{th}1}P_{d_{1}}\varphi_{1}\chi_{4}} e^{\chi_{4} - \frac{a\gamma_{\text{th}1}N_{0}}{\beta_{1}Pd_{h_{1}}^{-\partial}\varphi_{1}}} \text{Ei}(-\chi_{4}), 0 < \beta_{1} < u_{1} \\ 1 + \sum_{a=1}^{K} \sum_{b=1}^{K} {K \choose a} {K \choose b} (-1)^{a+b-2} \frac{(\beta_{2} - \gamma_{\text{th}2}\beta_{1})d_{h_{1}}^{-\partial}P\varphi_{1}\chi_{5}}{a\gamma_{\text{th}2}P_{d_{1}}\varphi_{1} + (\beta_{2} - \gamma_{\text{th}2}\beta_{1})d_{h_{1}}^{-\partial}P\varphi_{1}} e^{\chi_{5} - \frac{a\gamma_{\text{th}2}N_{0}}{(\beta_{2} - \gamma_{\text{th}2}\beta_{1})d_{h_{1}}^{-\partial}P\varphi_{1}}} \text{Ei}(-\chi_{5}), u_{1} < \beta_{1} < u_{2}. \end{cases}$$

$$(14)$$

E. Extended Case of RIS With Random Phase Shift

We consider the RIS relying on random phase shift with ϖ_i 's in $\Gamma = \text{diag}(e^{j\overline{\omega}_1}, \dots, e^{j\overline{\omega}_M})$ are uniformly and randomly distributed in $\varpi_i \in [-\pi, \pi]$, where ϖ_i are the phase shifts induced by the RIS. Then, we refer to reevaluate the performance of user D_2 . Assume the channel between source and RIS is $g_{s,ki} \sim CN(0, \varphi_{sr}I_M)$; between RIS and D_2 is $g_{r,i} \sim CN(0, \varphi_{rd}I_M)$, where φ_{sr} and φ_{rd} are large-scale-fading coefficients [44], [45]. The large-scalefading coefficients [dB] are modeled, similar to [46], by $\varphi_w(dB) = G_{tr} + G_{re} + 10\partial \log_{10}(d_w/1m) - 30 + \lambda_w$, where $w = \{sr, rd_2\}; G_{tr} \text{ and } G_{re} \text{ are the antenna gain at the }$ transmitter and receiver, respectively; the shadow fading is $\dot{\tau}_w$ [44]. If the source is transmitting an information symbol $E[|x_n|^2] = 1$ and assuming first-order reflection from RIS only, the received complex base-band signal at D_2 is formulated by [36], [44]

$$y_{2,r} = \frac{\tau g_{s,k^*i}^H g_{r,i}^H}{\sqrt{d_{sr}^{\partial} d_{rd_2}^{\partial}}} \Gamma x + \frac{\theta v_{k^*} l_2}{\sqrt{(d_v + d_{l_2})^{\partial}}} xs + \sqrt{P_{d_2}} g_2 x_{d_2} + \sigma_2$$

$$= \underbrace{\frac{\tau g_{s,k^*i}^H g_{r,i}^H}{\sqrt{d_{sr}^{\partial} d_{rd_2}^{\partial}}} \Gamma \sqrt{P \beta_2} x_2 + \underbrace{\frac{\tau g_{s,k^*i}^H g_{r,i}^H}{\sqrt{d_{sr}^{\partial} d_{rd_2}^{\partial}}} \Gamma \sqrt{P \beta_1} x_1}_{\text{signal}} \underbrace{\frac{\tau g_{s,k^*i}^H g_{r,i}^H}{\sqrt{d_{sr}^{\partial} d_{rd_2}^{\partial}}} \Gamma \sqrt{P \beta_1} x_1}_{\text{intra-cluster interference}}$$

$$+ \underbrace{\sqrt{P_{d_2} g_2 x_{d_2}}}_{\text{interference from } BS_2} + \underbrace{\frac{\theta v_{k^*} l_2}{\sqrt{(d_v + d_{l_2})^{\partial}}} xs + \sigma_2}_{\text{(19)}}$$

By treating the other signal components as interference, D_2 only decodes its own message x_2 . To decode signal x_2 , the SINR is formulated by

$$\gamma_{2,k^*r} = \frac{\beta_2 \tau P d_{sr}^{-\partial} d_{rd_2}^{-\partial} Z_{k^*}^2}{\beta_1 \tau P d_{sr}^{-\partial} d_{rd_2}^{-\partial} Z_{k^*}^2 + P \wp_2 |v_{k^*}|^2 |l_2|^2 + P_{d2} |g_2|^2 + N_0}$$
(20)

where $Z_{k^*}=g^H_{s,k^*i}g^H_{r,i}$, as $M\to\infty$ it holds that $Z_k\sim CN(0,M\varphi_{sr}\varphi_{rd_2})$ [45].

Similar to (15), the outage probability of D_2 is expressed as [44]

$$OP_{2,r} = 1 - \underbrace{\Pr(\gamma_{2,k^*r} \ge \gamma_{\text{th}2})}_{\Psi_{2,r}}.$$
 (21)

By relying on (21), we have (22), shown at the bottom of the next page.

We continue to leverage results from [33, eq. (3.352.4)] and apply some polynomial expansion manipulations, $\Psi_{2,r}$ is further computed by

$$\Psi_{2,r} = -\sum_{a=1}^{K} \sum_{b=1}^{K} {K \choose a} {K \choose b} (-1)^{a+b-2}$$

$$\times \frac{\chi_7(\beta_2 - \gamma_{\text{th}2}\beta_1) \tau P d_{sr}^{-\partial} d_{rd_2}^{-\partial} M \varphi_{sr} \varphi_{rd_2}}{a \gamma_{\text{th}2} P_{d2} \varphi_{g,2} + (\beta_2 - \gamma_{\text{th}2}\beta_1) \tau P d_{sr}^{-\partial} d_{rd_2}^{-\partial} M \varphi_{sr} \varphi_{rd_2}}$$

$$\times e^{\chi_7 - \frac{a \gamma_{\text{th}2} N_0}{(\beta_2 - \gamma_{\text{th}2}\beta_1) \tau P d_{sr}^{-\partial} d_{rd_2}^{-\partial} M \varphi_{sr} \varphi_{rd_2}}} \text{Ei}(-\chi_7)$$
(23)

where $\chi_7 = ([(\beta_2 - \gamma_{\text{th}2}\beta_1)b\tau d_{sr}^{-\partial}d_{rd_2}^{-\partial}M\varphi_{sr}\varphi_{rd_2}]/[a\gamma_{\text{th}2}\wp_2\varphi_v\varphi_{l,2}]).$

$$\begin{split} &\Psi = \Pr(\gamma_{2k^*} \geq \gamma_{\text{th}2}) \\ &= \Pr\left(Q_{1k^*}^2 \geq \frac{\gamma_{\text{th}2}(P_{\delta^2}|v_{k^*}|^2|I_2|^2 + P_{d2}|g_2|^2 + N_0)}{(\beta_2 - \gamma_{\text{th}2}\beta_1)\tau P d_{sr}^{-\delta} d_{rd_2}^{-\delta}}\right) \\ &= \int_0^\infty \int_0^\infty \int_0^\infty \left(1 - F_{Q_{1k^*}^2} \left(\frac{\gamma_{\text{th}2}(P_{\delta^2}|x_{V}^2|+ P_{d2}|x_{V}^2|+ N_0)}{(\beta_2 - \gamma_{\text{th}2}\beta_1)\tau P d_{sr}^{-\delta} d_{rd_2}^{-\delta}}\right)\right) f_{|v_{k^*}|^2}(x) f_{|z_2|^2}(y) f_{|g_2|^2}(z) dx dy dz \\ &= \sum_{a=1}^K \sum_{b=1}^K {K \choose a} {K \choose b} (-1)^{a+b-2} \frac{b}{\varphi_{V} \varphi_{l,2} \varphi_{g,2}} e^{-\frac{\alpha \gamma_{\text{th}2}\beta_1}{(\beta_2 - \gamma_{\text{th}2}\beta_1)\tau P M d_{sr}^{-\delta} d_{rd_2}^{-\delta}}} \int_0^\infty \int_0^\infty \int_0^\infty e^{-\frac{\alpha \gamma_{\text{th}2} p_{2N}}{(\beta_2 - \gamma_{\text{th}2}\beta_1)\tau M d_{sr}^{-\delta} d_{rd_2}^{-\delta}}} e^{-\frac{bx}{\varphi_{V}}} \\ &\times e^{-\frac{\alpha \gamma_{\text{th}2} P_{d2} z}{(\beta_2 - \gamma_{\text{th}2}\beta_1)\tau P M d_{sr}^{-\delta} d_{rd_2}^{-\delta}}} \int_0^\infty e^{-\frac{\alpha \gamma_{\text{th}2} p_{2N}}{(\beta_2 - \gamma_{\text{th}2}\beta_1)\tau P M d_{sr}^{-\delta} d_{rd_2}^{-\delta}}} \int_0^\infty e^{-\frac{\alpha \gamma_{\text{th}2} p_{2N}}{(\beta_2 - \gamma_{\text{th}2}\beta_1)\tau P M d_{sr}^{-\delta} d_{rd_2}^{-\delta}}} \int_0^\infty e^{-\frac{\alpha \gamma_{\text{th}2} p_{2N}}{(\beta_2 - \gamma_{\text{th}2}\beta_1)\tau P M d_{sr}^{-\delta} d_{rd_2}^{-\delta}}} \int_0^\infty e^{-\frac{\alpha \gamma_{\text{th}2} p_{2N}}{(\beta_2 - \gamma_{\text{th}2}\beta_1)\tau P M d_{sr}^{-\delta} d_{rd_2}^{-\delta}}} \int_0^\infty e^{-\frac{\alpha \gamma_{\text{th}2} p_{2N}}{(\beta_2 - \gamma_{\text{th}2}\beta_1)\tau P M d_{sr}^{-\delta} d_{rd_2}^{-\delta}}} \int_0^\infty e^{-\frac{\alpha \gamma_{\text{th}2} p_{2N}}{(\beta_2 - \gamma_{\text{th}2}\beta_1)\tau P M d_{sr}^{-\delta} d_{rd_2}^{-\delta}}} \int_0^\infty e^{-\frac{\alpha \gamma_{\text{th}2} p_{2N}}{(\beta_2 - \gamma_{\text{th}2}\beta_1)\tau P M d_{sr}^{-\delta} d_{rd_2}^{-\delta}}} \int_0^\infty e^{-\frac{\alpha \gamma_{\text{th}2} p_{2N}}{(\beta_2 - \gamma_{\text{th}2}\beta_1)\tau P M d_{sr}^{-\delta} d_{rd_2}^{-\delta}}} \int_0^\infty e^{-\frac{\alpha \gamma_{\text{th}2} p_{2N}}{(\beta_2 - \gamma_{\text{th}2}\beta_1)\tau P M d_{sr}^{-\delta} d_{rd_2}^{-\delta}}} \int_0^\infty e^{-\frac{\alpha \gamma_{\text{th}2} p_{2N}}{(\beta_2 - \gamma_{\text{th}2}\beta_1)\tau P M d_{sr}^{-\delta} d_{rd_2}^{-\delta}}} \int_0^\infty e^{-\frac{\alpha \gamma_{\text{th}2} p_{2N}}{(\beta_2 - \gamma_{\text{th}2}\beta_1)\tau P M d_{sr}^{-\delta} d_{rd_2}^{-\delta}}} \int_0^\infty e^{-\frac{\alpha \gamma_{\text{th}2} p_{2N}}{(\beta_2 - \gamma_{\text{th}2}\beta_1)\tau P M d_{sr}^{-\delta} d_{rd_2}^{-\delta}}} \int_0^\infty e^{-\frac{\alpha \gamma_{\text{th}2} p_{2N}}{(\beta_2 - \gamma_{\text{th}2}\beta_1)\tau P M d_{sr}^{-\delta} d_{rd_2}^{-\delta}}} \int_0^\infty e^{-\frac{\alpha \gamma_{\text{th}2} p_{2N}}{(\beta_2 - \gamma_{\text{th}2}\beta_1)\tau P M d_{sr}^{-\delta} d_{rd_2}^{-\delta}}} \int_0^\infty e^{-\frac{\alpha \gamma_{\text{th}2} p_{2N}}{(\beta_2 - \gamma_{\text{th}2}\beta_1)\tau P M d_{$$

From (23) into (21), the closed-form expression for the outage probability at D_2 using random phase shift is given by

$$OP_{2,r} = 1 + \sum_{a=1}^{K} \sum_{b=1}^{K} {K \choose a} {K \choose b} (-1)^{a+b-2}$$

$$\times \frac{\chi_{7}(\beta_{2} - \gamma_{\text{th}2}\beta_{1})\tau P d_{sr}^{-\partial} d_{rd_{2}}^{-\partial} M \varphi_{sr} \varphi_{rd_{2}}}{a \gamma_{\text{th}2} P_{d2} \varphi_{g,2} + (\beta_{2} - \gamma_{\text{th}2}\beta_{1})\tau P d_{sr}^{-\partial} d_{rd_{2}}^{-\partial} M \varphi_{sr} \varphi_{rd_{2}}}$$

$$\times e^{\chi_{7} - \frac{a \gamma_{\text{th}2} N_{0}}{(\beta_{2} - \gamma_{\text{th}2}\beta_{1})\tau P d_{sr}^{-\partial} d_{rd_{2}}^{-\partial} M \varphi_{sr} \varphi_{rd_{2}}}}{\text{Ei}(-\chi_{7}).$$
(24)

F. Asymptotic Analysis

According to the analytical results in (14) and (16), we further explore the asymptotic expressions and the diversity order in the high SNR regime.

Corollary 1: The asymptotic expression for outage probability at D_1 are given as when the transmitted power P/N_0 goes to infinity.

1) With perfect SIC

$$OP_1^{\infty} = 1 + \sum_{a=1}^{K} \sum_{b=1}^{K} {K \choose a} {K \choose b} (-1)^{a+b-2} \chi_1^{\infty} e^{\chi_1^{\infty}} \text{Ei}(-\chi_1^{\infty})$$
(25)

where $\Omega_1^{\infty}=\max((\gamma_{\text{th}2}/[(\beta_2-\gamma_{\text{th}2}\beta_1)d_{h_1}^{-\partial}]),(\gamma_{\text{th}1}/[\beta_1d_{h_1}^{-\partial}]))$ and $\chi_1^{\infty}=(b\varphi_1/[a\Omega_1^{\infty}\wp_1\varphi_\nu\varphi_{l,1}]).$ 2) With imperfect SIC, $OP_{1,ip}^{\infty}$ is expressed as (26), shown

at the bottom of the page.

Corollary 2: By looking at (11), when $P/N_0 \rightarrow \infty$, the asymptotic expression for outage probability at BD for BackCom RIS-NOMA in the high SNR region is given by

$$OP_{\text{BD}}^{\infty} = 1 - \sum_{a=1}^{K} \sum_{b=1}^{K} {K \choose a} {K \choose b} (-1)^{a+b-2} \times \frac{1}{\varphi_{g,1} \left(\frac{\chi_2 \gamma_{thb} \frac{P_{d1}}{N_0}}{\frac{P}{N_0} \wp_1} + \frac{a \Omega_1^{\infty} \frac{P_{d1}}{N_0}}{\frac{P}{N_0} \varphi_1} + \frac{1}{\varphi_{g,1}} \right)}$$

$$\times \frac{b\varphi_{1}}{a\Omega_{1}^{\infty}\wp_{1}\varphi_{\nu}\varphi_{l,1} + b\varphi_{1}} e^{-\frac{\chi_{2}\gamma_{hh}N_{0}}{P\wp_{1}} - \frac{a\Omega_{1}^{\infty}N_{0}}{P\wp_{1}}}$$

$$= 1 - \sum_{a=1}^{K} \sum_{b=1}^{K} {K \choose a} {K \choose b} (-1)^{a+b-2}$$

$$\times \frac{b\varphi_{1}}{a\Omega_{1}^{\infty}\wp_{1}\varphi_{\nu}\varphi_{l,1} + b\varphi_{1}} \tag{27}$$

where $([(\chi_2 \gamma_{thb} [P_{d1}/N_0])/([P/N_0] \wp_1)] + ([a\Omega_1^{\infty} (P_{d1}/N_0)])/([P/N_0) \wp_1)] + (1/\wp_{g,1}) \rightarrow (1/\wp_{g,1}),$ and $\begin{array}{l} /[(P/N_0)\varphi_1]) + (1/\varphi_{g,1})) \\ e^{-([\chi_2\gamma_{thb}N_0]/P\wp_1) - ([a\Omega_1^\infty N_0]/P\varphi_1)} \to 1 \end{array}$

Corollary 3: In case of $P/N_0 \to \infty$, the asymptotic expression for outage probability at D_2 in the high SNR region is given by the following.

1) Without random phase shift

$$OP_2^{\infty} = 1 + \sum_{a=1}^K \sum_{b=1}^K {K \choose a} {K \choose b} (-1)^{a+b-2} \chi_6 e^{\chi_6} \text{Ei}(-\chi_6).$$
(28)

2) With random phase shift

$$OP_{2,r}^{\infty} = 1 + \sum_{a=1}^{K} \sum_{b=1}^{K} {K \choose a} {K \choose b} (-1)^{a+b-2} \chi_7 e^{\chi_7} \text{Ei}(-\chi_7).$$
(29)

Proof: See Appendix E.

Remark 3: In principle, the asymptotic expressions showing outage behavior can be used to explore the diversity order, which is considered as a crucial performance metric to evaluate how fast the outage probability decreases with high transmit SNR. Conventionally, the diversity order presented in the next section refers to an asymptotic quantity when the transmit SNR goes to infinity.

G. Diversity Order

To look at insights of such outage behavior, we need to know the diversity order. Once can define the diversity order as

$$d_{\text{div}} = -\lim_{\overline{\rho} \to \infty} \frac{\log OP^{\infty}}{\log \overline{\rho}}$$
 (30)

$$\Psi_{2,r} = \Pr(\gamma_{2,k^*r} \geq \gamma_{\text{th}2}) \\
= \Pr\left(Z_{k^*}^2 \geq \frac{\gamma_{\text{th}2}(P\wp_2|\nu_{k^*}|^2|l_2|^2 + P_{d2}|g_2|^2 + N_0)}{(\beta_2 - \gamma_{\text{th}2}\beta_1)\tau P d_{sr}^{-\partial} d_{rd_2}^{-\partial}}\right) \\
= \sum_{a=1}^K \sum_{b=1}^K {K \choose a} {K \choose a} {K \choose b} (-1)^{a+b-2} \frac{(\beta_2 - \gamma_{\text{th}2}\beta_1)\tau P d_{sr}^{-\partial} d_{rd_2}^{-\partial} M \varphi_{sr} \varphi_{rd_2}}{\varphi_{l,2} \left(a\gamma_{\text{th}2} P_{d2} \varphi_{g,2} + (\beta_2 - \gamma_{\text{th}2}\beta_1)\tau P d_{sr}^{-\partial} d_{rd_2}^{-\partial} M \varphi_{sr} \varphi_{rd_2}\right)} e^{-\frac{a\gamma_{\text{th}2}N_0}{(\beta_2 - \gamma_{\text{th}2}\beta_1)\tau P d_{sr}^{-\partial} d_{rd_2}^{-\partial} M \varphi_{sr} \varphi_{rd_2}}} \\
\times \int_0^\infty \frac{(\beta_2 - \gamma_{\text{th}2}\beta_1)b\tau d_{sr}^{-\partial} d_{rd_2}^{-\partial} M \varphi_{sr} \varphi_{rd_2}}{a\gamma_{\text{th}2}\wp_2 \varphi_{\nu} y + (\beta_2 - \gamma_{\text{th}2}\beta_1)b\tau d_{sr}^{-\partial} d_{rd_2}^{-\partial} M \varphi_{sr} \varphi_{rd_2}} e^{-\frac{y}{\varphi_{l,2}}} dy. \tag{22}$$

$$OP_{1,ip}^{\infty} = \begin{cases} 1 + \sum_{a=1}^{K} \sum_{b=1}^{K} \sum_{c=1}^{K} {K \choose a} {K \choose b} {K \choose c} (-1)^{a+b+c-3} \frac{b\beta_1\varphi_1\chi_4e^{\chi_4} \text{Ei}(-\chi_4)}{a\gamma_{\text{th}1}\beta_2k_1\varphi_{ip} + b\beta_1\varphi_1}, 0 < \beta_1 < u_1 \\ 1 + \sum_{a=1}^{K} \sum_{b=1}^{K} {K \choose a} {K \choose b} (-1)^{a+b-2} \chi_5 e^{\chi_5} \text{Ei}(-\chi_5), u_1 < \beta_1 < u_2. \end{cases}$$

$$(26)$$

where $\overline{\rho}$ stands for the SNR of the source, and OP^{∞} is the value of outage probability that we are considering. It is worth noting that we have $\lim_{\rho \to \infty} e^{-(x/\rho)} \simeq 1 - (x/\rho)$, then each user experiences zero diversity order problem in the considered system, which leads to saturation of outage behavior owing to the existence of other parameters rather than SNR.

Remark 4: From the diversity order result, we can see that when the transmit SNR at the source (BS) goes to infinity, the curves of outage probability tend to become a constant. It can be explained that the corresponding SINRs to detect the signals at the users increase to provide better outage behavior, but this still depends on other main factors, for example, noise and interference levels. It means that the considered systems experience the limitation at high SNR of the BS regardless of advanced techniques applied to such system.

H. System Throughput Analysis

In this section, we derive and evaluate the throughput of the considered system. The system throughput can be defined as the total information being successfully transmitted and decoded with a constant data rate per unit time. Relying on the achievable outage probabilities obtained in (9), (11), (14), and (16), the system throughput can be expressed in the delay-limited transmission mode as

$$TP_S = (1 - OP_{\dagger})R_1 + (1 - OP_2)R_2 + (1 - OP_{BD})R_s$$
 (31)
where $\dagger \in (1; 1, ip)$.

IV. ERGODIC CAPACITY ANALYSIS

The ergodic capacity is another important performance metric when the rates of users are determined by their channel conditions [3]. Hence, in this section, we analyze the ergodic rates for all relevant transmissions in the considered system to complete the analysis of the system performance, which would provide important design guidelines.

A. Ergodic Capacity of D_1

In this section, we provide the ergodic capacity of D_1 . On the condition that D_1 detects x_2 perfectly, the ergodic capacity of D_1 is given by

$$R_{D_1} = \mathrm{E}(\log_2(1 + \gamma_{1k^*}))$$

$$= \frac{1}{\ln 2} \int_0^{+\infty} \frac{1 - F_{\gamma_{1k^*}}(l)}{1 + l} dl.$$
 (32)

 $F_{\gamma_{1k^*}}(l)$ is calculated similarly to (57), when $F_{\gamma_{1k^*}}(l)$ is given by

$$F_{\gamma_{lk^*}}(l) = 1 + \sum_{a=1}^{K} \sum_{b=1}^{K} {K \choose a} {K \choose b} (-1)^{a+b-2} \frac{\beta_1 P d_{h_1}^{-\partial} \varphi_1}{a l P_{d1} \varphi_{g,1} + \beta_1 P d_{h_1}^{-\partial} \varphi_1} \times \frac{I_1}{l} e^{\frac{I_1}{l} - \frac{a l N_0}{\beta_1 P d_{h_1}^{-\partial} \varphi_1}} \text{Ei} \left(-\frac{I_1}{l}\right)$$
(33)

where $I_1 = ([b\beta_1 d_{h_1}^{-\partial} \varphi_1]/[a\wp_1 \varphi_{\nu} \varphi_{l,1}]).$

From (33) into (32), R_{D_1} can be rewritten as

$$R_{D_{1}} = \frac{1}{\ln 2} \int_{0}^{+\infty} \sum_{a=1}^{K} \sum_{b=1}^{K} {K \choose a} {K \choose b} (-1)^{a+b-2} \times \frac{-I_{1} \beta_{1} P d_{h_{1}}^{-\partial} \varphi_{1}}{l \left(al P_{d1} \varphi_{g,1} + \beta_{1} P d_{h_{1}}^{-\partial} \varphi_{1}\right) (1+l)} e^{i \frac{1}{l} - \frac{al N_{0}}{\beta_{1} P d_{h_{1}}^{-\partial} \varphi_{1}}} \operatorname{Ei} \left(-\frac{I_{1}}{l}\right) dl.$$
(34)

From (34), it is difficult to obtain an accurate closed-form expression for R_{D_1} , and thus we assume the case where Q is large. Then, we have

$$R_{D_{1}} \approx \frac{1}{\ln 2} \int_{0}^{Q} \sum_{a=1}^{K} \sum_{b=1}^{K} {K \choose a} {K \choose b} (-1)^{a+b-2} \times \frac{-I_{1} \beta_{1} P d_{h_{1}}^{-\partial} \varphi_{1}}{l \left(a l P_{d 1} \varphi_{g, 1} + \beta_{1} P d_{h_{1}}^{-\partial} \varphi_{1}\right) (1+l)} e^{\frac{l_{1}}{l} - \frac{a l N_{0}}{\beta_{1} P d_{h_{1}}^{-\partial} \varphi_{1}}} \operatorname{Ei}\left(-\frac{I_{1}}{l}\right) dl.$$
(35)

Applying the Gaussian–Chebyshev quadrature [33], R_{D_1} is given by

$$R_{D_{1}} \approx \sum_{a=1}^{K} \sum_{b=1}^{K} \sum_{n=1}^{N} {K \choose a} {K \choose b} (-1)^{a+b-2} \frac{-bQ\pi \beta_{1} \beta_{1} P d_{h_{1}}^{-\partial} \varphi_{1} d_{h_{1}}^{-\partial} \varphi_{1}}{Na \wp_{1} \varphi_{\nu} \varphi_{l,1} \ln 2} \times \frac{\sqrt{1 - t_{i}^{2}}}{(Qt_{i} + Q) \left(\Lambda_{1} a P_{d1} \varphi_{g,1} + \beta_{1} P d_{h_{1}}^{-\partial} \varphi_{1} \right) (1 + \Lambda_{1})} \times e^{\Lambda_{2} - \frac{(Qt_{i} + Q)aN_{0}}{2\beta_{1} P d_{h_{1}}^{-\partial} \varphi_{1}}} \operatorname{Ei}(-\Lambda_{2})$$
(36)

where $\Lambda_1 = ([Qt_i + Q]/2)$, $\Lambda_2 = [2I_1/(Qt_i + Q)]$, $t_i = \cos[((2n-1)\pi)/2N]$, N is an accuracy–complexity tradeoff parameter.

B. Ergodic Capacity of BD

The rate of BD can be written as

$$R_{\text{BD}} = \text{E}\left(\log_2(1 + \gamma_{sk^*})\right) = \frac{1}{\ln 2} \int_0^{+\infty} \frac{1 - F_{\gamma_{sk^*}}(l)}{1 + l} dl.$$
 (37)

 $F_{\gamma_{sl}*}(l)$ can be calculated as

$$F_{\gamma_{sk^*}}(l) = 1 - \Pr\left(|v_{k^*}|^2 \ge \frac{l(P_{d1}|g_1|^2 + N_0)}{P_{\varnothing 1}|l_1|^2}\right)$$

$$= 1 - \int_0^\infty \int_0^\infty \left\{1 - F_{|v_{k^*}|^2} \left[\frac{l(P_{d1}x + N_0)}{P_{\varnothing 1}y}\right]\right\}$$

$$\times f_{|g_1|^2}(x)f_{|l_1|^2}(y)dxdy$$

$$= 1 - \sum_{a=1}^K {K \choose a}(-1)^{a-1} \int_0^\infty \frac{P_{\varnothing 1}\varphi_{\nu}y}{\varphi_{l,1}(alP_{d1}\varphi_{g,1} + P_{\varnothing 1}\varphi_{\nu}y)}$$

$$\times e^{-\frac{alN_0}{P_{\varnothing 1}\varphi_{\nu}y} - \frac{y}{\varphi_{l,1}}}dy. \tag{38}$$

Similar to (35), when Q is a large value and applying the Gaussian–Chebyshev quadrature, we have

$$F_{\gamma_{sk^*}}(l) \approx 1 - \sum_{a=1}^{K} \sum_{n=1}^{N} {K \choose a} (-1)^{a-1} \frac{\pi Q}{2N\varphi_{l,1}}$$

$$\times \frac{\sqrt{1-t_{i}^{2}}P\wp_{1}\varphi_{v}(Qt_{i}+Q)}{2alP_{d1}\varphi_{g,1}+P\wp_{1}\varphi_{v}(Qt_{i}+Q)}e^{-\frac{2alN_{0}}{P\wp_{1}\varphi_{v}(Qt_{i}+Q)}-\frac{Qt_{i}+Q}{2\varphi l,1}}.$$
(39)

From (39) into (37), we have

$$R_{\rm BD} \approx \sum_{a=1}^{K} \sum_{n=1}^{N} {K \choose a} (-1)^{a-1} \frac{\sqrt{1 - t_i^2} \pi Q}{2N \varphi_{l,1} \ln 2} \int_{0}^{+\infty} \frac{1}{1 + l} \times \frac{P \wp_1 \varphi_{\nu}(Qt_i + Q)}{2al P_{d1} \varphi_{g,1} + P \wp_1 \varphi_{\nu}(Qt_i + Q)} e^{-\frac{2al N_0}{P \wp_1 \varphi_{\nu}(Qt_i + Q)} - \frac{Qt_i + Q}{2\varphi_{l,1}}} dl.$$
(40)

It is difficult to obtain a closed-form expression for (40). Thus, we again use the approximation in (35) and obtain

$$R_{\text{BD}} \approx \sum_{a=1}^{K} \sum_{n=1}^{N} {K \choose a} (-1)^{a-1} \frac{\sqrt{1 - t_i^2} \pi Q}{2N\varphi_{l,1} \ln 2} \int_{0}^{Q} \frac{1}{1 + l} \times \frac{P\wp_1 \varphi_{\nu}(Qt_i + Q)}{2alP_{d1} \varphi_{g,1} + P\wp_1 \varphi_{\nu}(Qt_i + Q)} e^{-\frac{2alN_0}{P\wp_1 \varphi_{\nu}(Qt_i + Q)} - \frac{Qt_i + Q}{2\varphi_{l,1}}} dl.$$
(41)

Applying the Gaussian-Chebyshev quadrature [33], $R_{\rm BD}$ is given by

$$R_{\text{BD}} \approx \sum_{a=1}^{K} \sum_{u=1}^{U} \sum_{n=1}^{N} {K \choose a} (-1)^{a-1} \frac{\sqrt{1 - w_i^2} \sqrt{1 - t_i^2 \pi \pi QQ}}{2UN\varphi_{l,1} \ln 2} \times \frac{P\wp_1 \varphi_v(Qt_i + Q)}{(2 + Qw_i + Q) [(Qw_i + Q)aP_{d1}\varphi_{g,1} + P\wp_1 \varphi_v(Qt_i + Q)]} \times e^{-\frac{aN_0(Qw_i + Q)}{P\wp_1 \varphi_v(Qt_i + Q)} - \frac{2t_i + Q}{2\varphi_{l,1}}}$$
(42)

where $w_i = \cos[((2u-1)\pi)/2U]$, U is an accuracy– complexity tradeoff parameter.

C. Ergodic Capacity of D₁ With Imperfect SIC

The ergodic capacity of D_1 with imperfect SIC can be written as

$$R_{D_1,ip} = E(\log_2(1 + \gamma_{1k^*,ip}))$$

$$= \frac{1}{\ln 2} \int_0^{+\infty} \frac{1 - F_{\gamma_{1k^*,ip}}(l)}{1 + l} dl.$$
 (43)

Similar to (64), shown at the bottom of p. 16, $F_{\gamma_{1k}*_{in}}(l)$ is

$$F_{\gamma_{lk^*,ip}}(l) = 1 - \sum_{a=1}^{K} \sum_{b=1}^{K} \sum_{c=1}^{K} {K \choose a} {K \choose b} {K \choose c} (-1)^{a+b+c-3}$$

$$Q \text{ is a large number and applying the Gaussian-Chebyst quadrature [33], we have}$$

$$\times \frac{-bc\beta_1\beta_1\beta_1Pd_{h_1}^{-\partial}d_{h_1}^{-\partial}\varphi_1\varphi_1}{al\wp_1\varphi_\nu\varphi_{l,1}(al\beta_2k_1\varphi_{lp} + b\beta_1\varphi_1)\Big(alP_{d1}\varphi_{g,1} + \beta_1Pd_{h_1}^{-\partial}\varphi_1\Big)}$$

$$\times e^{\frac{c\beta_1d_{h_1}^{-\partial}\varphi_1}{al\wp_1\varphi_\nu\varphi_{l,1}} - \frac{alN_0}{\beta_1Pd_{h_1}^{-\partial}\varphi_1}} \text{Ei}\Big(-\frac{c\beta_1d_{h_1}^{-\partial}\varphi_1}{al\wp_1\varphi_\nu\varphi_{l,1}}\Big). \tag{44}$$

$$F_{\gamma_{2k^*}}(l) \approx 1 - \sum_{a=1}^{K} \sum_{b=1}^{K} \sum_{n=1}^{K} {K \choose a} {K \choose b} {K \choose b} {K \choose b} {K \choose a} e^{-\frac{l}{2}} \frac{1}{N\varphi_{l,2}} e^{-\frac{l}{2}} \frac{1}{N\varphi_{l,2}} e^{-\frac{l}{2}} \frac{1}{N\varphi_{l,2}} e^{-\frac{l}{2}} e^{-\frac{l}{2}} \frac{1}{N\varphi_{l,2}} e^{-\frac{l}{2}} \frac{1}{$$

Using (44) into (43), it is difficult to obtain an accurate closed-form expression for the ergodic capacity of D_1 with imperfect SIC, and thus, for Q is a large number, $R_{D_1,ip}$ is

approximated by

$$R_{D_{1},ip}$$

$$\approx \sum_{a=1}^{K} \sum_{b=1}^{K} \sum_{c=1}^{K} {K \choose a} {K \choose b} {K \choose c} (-1)^{a+b+c-3} \frac{1}{\ln 2}$$

$$\times \int_{0}^{Q} \frac{-bc\beta_{1}\beta_{1}\beta_{1}Pd_{h_{1}}^{-\partial}d_{h_{1}}^{-\partial}q_{h_{1}}\varphi_{1}\varphi_{1}}{al\wp_{1}\varphi_{v}\varphi_{l,1}\left(al\beta_{2}k_{1}\varphi_{ip}+b\beta_{1}\varphi_{1}\right)\left(alP_{d1}\varphi_{g,1}+\beta_{1}Pd_{h_{1}}^{-\partial}\varphi_{1}\right)(1+l)}$$

$$\times e^{\frac{c\beta_{1}d_{h_{1}}^{-\partial}\varphi_{1}}{al\wp_{1}\varphi_{v}\varphi_{l,1}} - \frac{alN_{0}}{\beta_{1}Pd_{h_{1}}^{-\partial}\varphi_{1}}} \operatorname{Ei}\left(-\frac{c\beta_{1}d_{h_{1}}^{-\partial}\varphi_{1}}{al\wp_{1}\varphi_{v}\varphi_{l,1}}\right)dl. \tag{45}$$

Applying the Gaussian-Chebyshev quadrature [33], we can obtain $R_{D_1,ip}$ as

$$\Re \sum_{a=1}^{K} \sum_{b=1}^{K} \sum_{c=1}^{K} \sum_{n}^{N} {K \choose a} {K \choose b} {K \choose c} (-1)^{a+b+c-3} \\
\times \frac{-Q\pi bc\beta_1 \beta_1 \beta_1 P d_{h_1}^{-\partial} d_{h_1}^{-\partial} \varphi_1 \varphi_1 \varphi_1}{2N \ln 2} \\
\times \frac{\sqrt{1-t_i^2}}{\Lambda_1 a\wp_1 \varphi_\nu \varphi_{l,1} (\Lambda_1 a\beta_2 k_1 \varphi_{lp} + b\beta_1 \varphi_1) (\Lambda_1 aP_{d1} \varphi_{g,1} + \beta_1 P d_{h_1}^{-\partial} \varphi_1) (1+\Lambda_1)} \\
\times e^{\frac{c\beta_1 d_{h_1}^{-\partial} \varphi_1}{\Lambda_1 a\wp_1 \varphi_\nu \varphi_{l,1}} - \frac{\Lambda_1 aN_0}{\beta_1 P d_{h_1}^{-\partial} \varphi_1}} \operatorname{Ei} \left(-\frac{c\beta_1 d_{h_1}^{-\partial} \varphi_1}{\Lambda_1 a\wp_1 \varphi_\nu \varphi_{l,1}} \right).$$
(46)

D. Ergodic Capacity of D₂

The rate of D_2 can be written as

$$R_{D_2} = \mathrm{E}(\log_2(1 + \gamma_{2k^*}))$$

$$= \frac{1}{\ln 2} \int_0^{+\infty} \frac{1 - F_{\gamma_{2k^*}}(l)}{1 + l} dl.$$
 (47)

 $F_{\gamma_{2,k^*}}(l)$ is calculated similarly to (17), when $F_{\gamma_{2,k^*}}(l)$ is

$$F_{\gamma_{2k^*}}(l) = 1 - \sum_{a=1}^{K} \sum_{b=1}^{K} {K \choose a} {K \choose b} (-1)^{a+b-2} \frac{1}{\varphi_{l,2}}$$

$$\times \frac{(\beta_2 - l\beta_1)\tau PM d_{sr}^{-\partial} d_{rd_2}^{-\partial}}{alP_{d2}\varphi_{g,2} + (\beta_2 - l\beta_1)\tau PM d_{sr}^{-\partial} d_{rd_2}^{-\partial}}$$

$$\times \int_{0}^{\infty} \frac{(\beta_2 - l\beta_1)b\tau M d_{sr}^{-\partial} d_{rd_2}^{-\partial}}{al\wp_2\varphi_v y + (\beta_2 - l\beta_1)b\tau M d_{sr}^{-\partial} d_{rd_2}^{-\partial}}$$

$$\times e^{-\frac{alN_0}{(\beta_2 - l\beta_1)\tau PM d_{sr}^{-\partial} d_{rd_2}^{-\partial}} - \frac{y}{\varphi_{l,2}}} dy. \tag{48}$$

From (48), we find it is difficult to obtain an accurate closedform expression for $F_{\gamma_{2l}*}(l)$ and thus we assume that when Q is a large number and applying the Gaussian-Chebyshev quadrature [33], we have

$$\begin{split} F_{\gamma_{2k^*}}(l) &\approx 1 - \sum_{a=1}^K \sum_{b=1}^K \sum_{n=1}^N \binom{K}{a} \binom{K}{b} (-1)^{a+b-2} \frac{\sqrt{1-t_i^2} \pi Q}{N \varphi_{l,2}} \\ &\times \frac{(\beta_2 - l\beta_1) \tau P M d_{sr}^{-\partial} d_{rd_2}^{-\partial}}{a l P_{d2} \varphi_{g,2} + (\beta_2 - l\beta_1) \tau P M d_{sr}^{-\partial} d_{rd_2}^{-\partial}} \\ &\times \frac{(\beta_2 - l\beta_1) b \tau M d_{sr}^{-\partial} d_{rd_2}^{-\partial}}{a l \wp_2 \varphi_v (Q t_i + Q) + 2 (\beta_2 - l\beta_1) b \tau M d_{sr}^{-\partial} d_{rd_2}^{-\partial}} \end{split}$$

$$\times e^{-\frac{alN_0}{(\beta_2 - l\beta_1)\tau PMd_{sr}^{-\partial}d_{rd_2}^{-\partial}} - \frac{Qt_i + Q}{2\varphi_{l,2}}}.$$
(49)

From (49) into (47), R_{D_2} can given by

$$\begin{split} R_{D_{2}} &\approx \sum_{a=1}^{K} \sum_{b=1}^{K} \sum_{n=1}^{N} {K \choose a} {K \choose b} (-1)^{a+b-2} \frac{\sqrt{1-t_{i}^{2}}}{\ln 2} \\ &\times \int_{0}^{\beta_{2}/\beta_{1}} \frac{\pi Q}{(1+l)N\varphi_{l,2}} \frac{(\beta_{2}-l\beta_{1})\tau PMd_{sr}^{-\partial}d_{rd_{2}}^{-\partial}}{alP_{d2}\varphi_{g,2} + (\beta_{2}-l\beta_{1})\tau PMd_{sr}^{-\partial}d_{rd_{2}}^{-\partial}} \\ &\times \frac{(\beta_{2}-l\beta_{1})b\tau Md_{sr}^{-\partial}d_{rd_{2}}^{-\partial}}{al\wp_{2}\varphi_{v}(Qt_{i}+Q) + 2(\beta_{2}-l\beta_{1})b\tau Md_{sr}^{-\partial}d_{rd_{2}}^{-\partial}} \\ &\times e^{-\frac{alN_{0}}{(\beta_{2}-l\beta_{1})\tau PMd_{sr}^{-\partial}d_{rd_{2}}^{-\partial}}{2l}} \frac{-\frac{Qt_{i}+Q}{2\varphi_{i,2}}}{dl}. \end{split}$$
(50)

Applying the Gaussian-Chebyshev quadrature [33], we have

$$R_{D_{2}} = \sum_{a=1}^{K} \sum_{b=1}^{K} \sum_{u=1}^{X} \sum_{n=1}^{N} {n \choose a} {n \choose b} (-1)^{a+b-2}$$

$$\times \frac{\sqrt{1 - w_{i}^{2}} \sqrt{1 - t_{i}^{2}} \pi \pi Q \beta_{2}}{(1 + \Lambda_{3}) 2 \beta_{1} U N \varphi_{i,2} \ln 2} \frac{(\beta_{2} - \Lambda_{3} \beta_{1}) \tau P M d_{sr}^{-\partial} d_{rd_{2}}^{-\partial}}{\Lambda_{3} a P_{d2} \varphi_{g,2} + (\beta_{2} - \Lambda_{3} \beta_{1}) \tau P M d_{sr}^{-\partial} d_{rd_{2}}^{-\partial}}$$

$$\times \frac{(\beta_{2} - \Lambda_{3} \beta_{1}) b \tau M d_{sr}^{-\partial} d_{rd_{2}}^{-\partial}}{\Lambda_{3} a \wp_{2} \varphi_{v} (Q t_{i} + Q) + 2 (\beta_{2} - \Lambda_{3} \beta_{1}) b \tau M d_{sr}^{-\partial} d_{rd_{2}}^{-\partial}}$$

$$\times e^{-\frac{\Lambda_{3} a N_{0}}{(\beta_{2} - \Lambda_{3} \beta_{1}) \tau P M d_{sr}^{-\partial} d_{rd_{2}}^{-\partial}}{2 \varphi_{i,2}} - \frac{Q t_{i} + Q}{2 \varphi_{i,2}}}$$
(51)

where $\Lambda_3 = ([\beta_2 w_i + \beta_2]/2\beta_1)$.

E. Ergodic Capacity of D2 With Random Phase Shift

Similar to (47), the ergodic capacity of D_2 with random phase shift is given by

$$R_{D_{2}r} = \sum_{a=1}^{K} \sum_{b=1}^{K} \sum_{u=1}^{U} \sum_{n=1}^{N} {K \choose a} {K \choose b} (-1)^{a+b-2}$$

$$\times \frac{\sqrt{1 - w_{i}^{2}} \sqrt{1 - t_{i}^{2}} \pi \pi Q \beta_{2}}{(1 + \Lambda_{3}) 2 \beta_{1} U N \varphi_{l,2} \ln 2}$$

$$\times \frac{(\beta_{2} - \Lambda_{3} \beta_{1}) \tau P M \varphi_{sr} \varphi_{rd_{2}} d_{sr}^{-\partial} d_{rd_{2}}^{-\partial}}{\Lambda_{3} a P_{d2} \varphi_{g,2} + (\beta_{2} - \Lambda_{3} \beta_{1}) \tau P M \varphi_{sr} \varphi_{rd_{2}} d_{sr}^{-\partial} d_{rd_{2}}^{-\partial}}$$

$$\times \frac{(\beta_{2} - \Lambda_{3} \beta_{1}) \tau P M \varphi_{sr} \varphi_{rd_{2}} d_{sr}^{-\partial} d_{rd_{2}}^{-\partial}}{\Lambda_{3} a \& \rho_{2} \varphi_{v} (Q t_{i} + Q) + 2(\beta_{2} - \Lambda_{3} \beta_{1}) b \tau M \varphi_{sr} \varphi_{rd_{2}} d_{sr}^{-\partial} d_{rd_{2}}^{-\partial}}$$

$$\times e^{-\frac{\Lambda_{3} a N_{0}}{(\beta_{2} - \Lambda_{3} \beta_{1}) \tau P M \varphi_{sr} \varphi_{rd_{2}} d_{sr}^{-\partial} d_{rd_{2}}^{-\partial}}{2 \varphi_{l,2}}}.$$
(52)

V. COMPARISON BETWEEN THEORETICAL AND NUMERICAL RESULTS

In this section, numerical results are presented to evaluate the considered BackCom NOMA-RIS system. The main parameters can be mentioned in Table III, except for specific cases. In what follows, we provide the outage probability, throughput, and ergodic capacity performance and present how BackCom NOMA-RIS outperforms the benchmark systems.

TABLE III
MAIN PARAMETERS FOR OUR SIMULATIONS

Description	NT-4-4*	X7-1
Parameters	Notation	Values
Power coefficients	$\{\beta_1,\beta_2\}$	$\{0.3, 0.7\}$
Target rate for x_1 and x_2	$R_1 = R_2$	1 (BPCU)
The target rate for BD	R_s	0.1 (BPCU)
A complex reflection coef-	θ	0.5
ficient		
The RIS attenuation factor	au	0.4
The level of residual inter-	k_1	0.8
ference associated with SIC		
Transmit SNR	$\{P/N_0, P_{d1}/N_0,$	$\{50(dB), 30(dB),$
	P_{d2}/N_0 }	10(dB)
Average powers	$\{\varphi_1 = \varphi_{l,2} =$	$\{1, 0.01\}$
	$\varphi_{l,2} = $	
	$\varphi_v = \varphi_{ip},$	
	$\varphi_{g,1} = \varphi_{g,2}$	
Number of reflecting ele-	M	1000
ments		
Number of transmission an-	K	3
tennas		
A large number	Q	1000
Accuracy-complexity trade-	Q N, U	200
off parameter		
The path loss	∂	1.5
The distances from BS to	d_{h_1}	7 (m)
D_1	n_1	. ,
The distances from BS to	d_v	5 (m)
BD	· ·	` '
The distances from BD to	d_{l_1}	5 (m)
D_1	ι_1	,
The distances from BD to	d_{l_2}	5 (m)
D_2	$-\iota_2$	- ()
The distances from BS to	d_{sr}	20 (m)
RIS	~sr	2 0 (III)
The distances from RIS to	d_{rd_2}	10 (m)
D_2	rd_2	10 (111)
The antenna gain at the	G_{tr}	1.5 (dBi) [44]
transmitter	~ .7	(abi) [i i]
The antenna gain at the re-	G_{re}	1 (dBi) [44]
ceiver	<i>∽1€</i>	, (abi) [11]
The shadow fading	λ_w	0 [44]
The shadow fading	$\wedge w$	البيا ن

A. Impacts of BD to Outage Performance

Fig. 2 illustrates the outage probabilities of User D_1 , User D_2 , and BD in the BackCom NOMA-RIS system and the BackCom SR system [32]. To confirm how exactly our findings are, the curves obtained from the analytical derivations are then matched with Monte Carlo simulations runs (averaging over 10⁶ times) thoroughly. By increasing the transmit average SNR at the BS, the outage probabilities can be reduced significantly. The outage performance of user D_2 is recognized as the best one among considered cases since more power assigned to D_2 . The impact of imperfect SIC to user D_1 can be seen clearly at the high SNR region. In addition, the asymptotic outage performance is exactly the same as the exact results at the high SNR regime which is consistent with theoretical analysis. The outage performance can be improved by adjusting θ to 0.3. We confirmed the saturation of such outage behavior as diversity order that was found in (30).

Fig. 3 demonstrates the effect of NOMA power allocation coefficients β_1 on the outage performance. Fortunately, we can find the optimal outage performance of user D_1 with perfect SIC since $\beta_1 = 0.3$ corresponds to the lowest value of outage probability. Similarly, the optimal point of user BD's outage

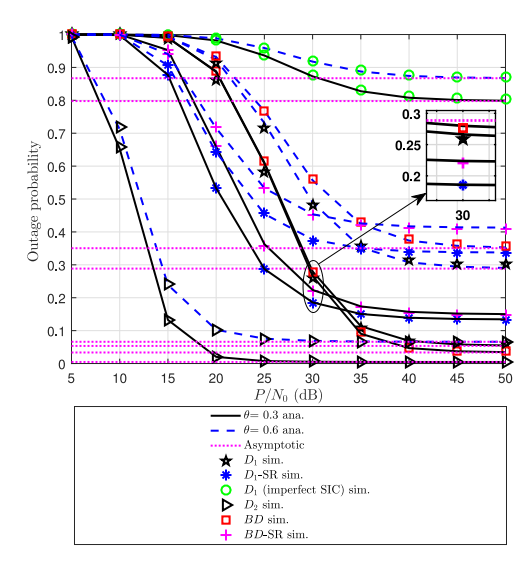


Fig. 2. Outage probability versus the transmit SNR P/N_0 at the source as changing θ in BackCom NOMA-RIS system in comparison with BackCom SR system [32].

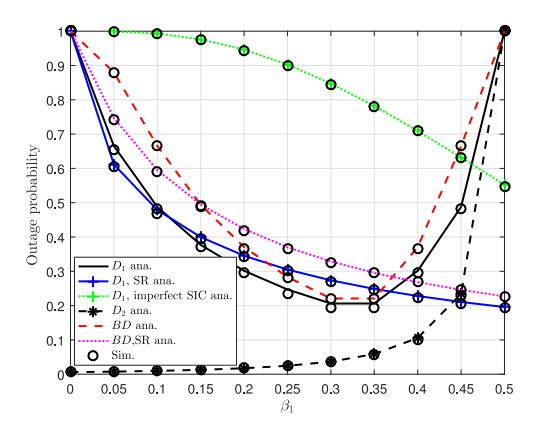


Fig. 3. Outage probability versus power allocation parameter β_1 for BackCom NOMA-RIS system in comparison with BackCom SR system [32].

probability can be reported. When β_1 varies from 0 to 0.5, user D_1 's outage probability with perfect SIC will improve, while user D_2 's outage probability will worsen. It can be explained that outage probabilities [e.g., (15)] depend on SINRs, while SINRs mostly rely on power allocation coefficients. It can be concluded that by adjusting the power allocation coefficients for the weak and strong users, the BS can make significantly influence the performance of such IoT user pair.

Fig. 4 illustrates how the outage performance varies under the adjustment of reflection parameter θ . In the BackCom NOMA-RIS system, the outage probabilities of two IoT devices become worse as θ increases. The main reason is that when θ increases, and the backscatter link leads to higher interference to the system, thereby leading to poor outage behavior. It is noted that the outage performance becomes worse when θ increases. Such situations are the same for both BackCom NOMA-RIS and BackCom SR systems. It can be explained that when θ is large, user D_1, D_2 find difficulty in decoding their signals.

Similarly, the outage probabilities for cases of user D_1 depend on the level of imperfect SIC, shown in Fig. 5. The

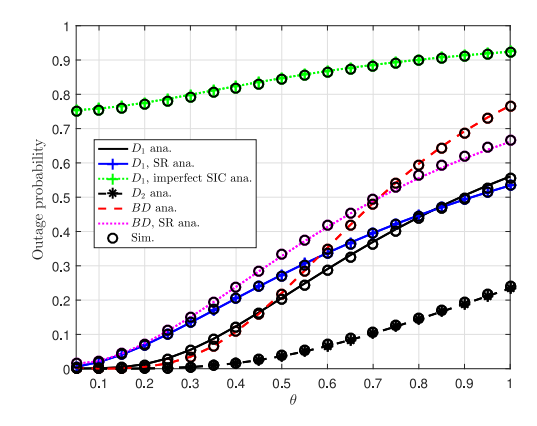


Fig. 4. Outage probability versus the reflection coefficient θ for BackCom NOMA-RIS system in comparison with BackCom SR system [32].

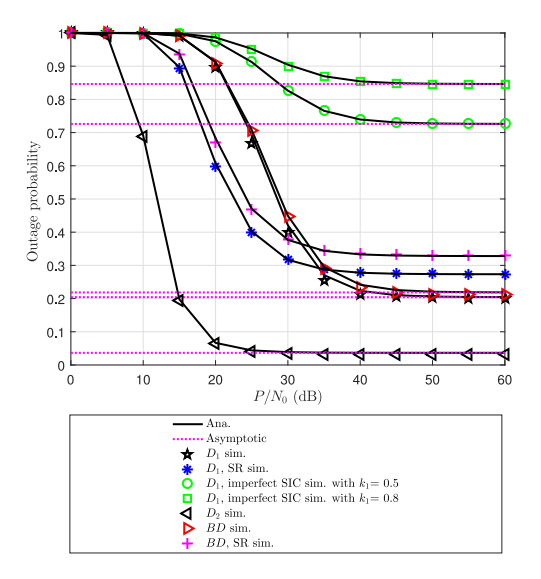


Fig. 5. Outage probability versus P/N_0 as changing k_1 .

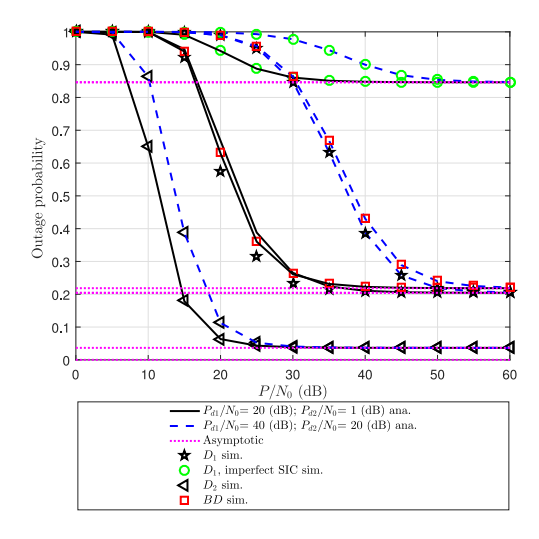


Fig. 6. Outage probability versus P/N_0 as changing $P_{d1}/N_0 = P_{d2}/N_0$.

trends of other performance curves are the similar as the analysis in the previous simulation.

In Fig. 6, we can see the impact of interference from coordinated BS to the system performance of the user under the

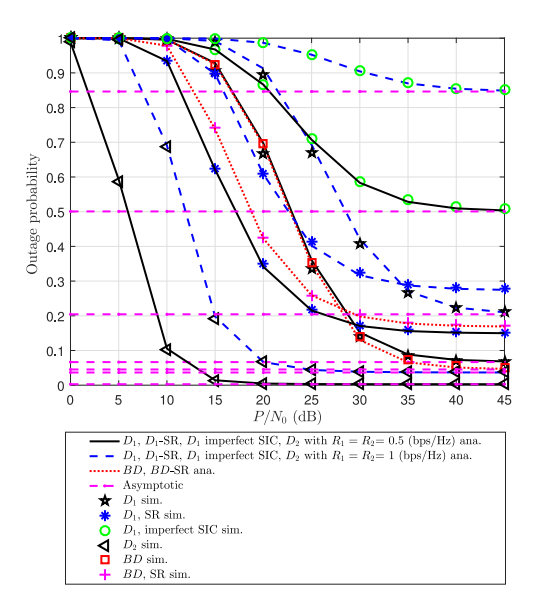


Fig. 7. Outage probabilities versus P/N_0 as changing R_1 , R_2 .

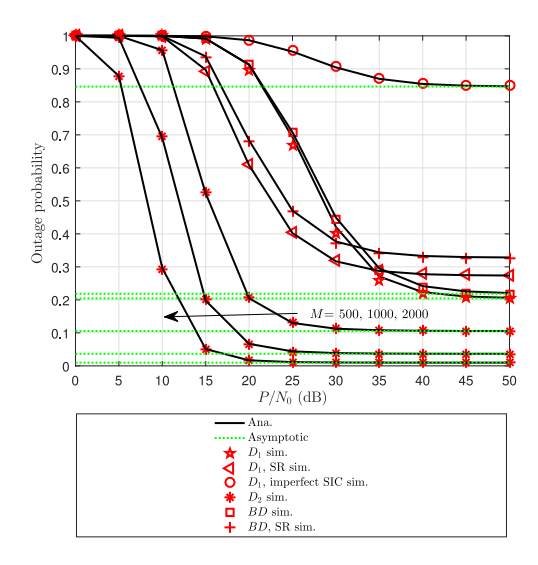


Fig. 8. Outage probability versus P/N_0 as changing M.

coverage of the main BS. The higher values of $P_{d1}/N_0 = P_{d2}/N_0$ lead to worse performance. This can be explained by the fact that more interference from nearby BS results in lower SINRs and then the outage probability becomes worse.

Similarly, in Fig. 7, it is intuitively seen that the outage probabilities for cases of all users depend on SINRs, while such SINRs are further decided by the corresponding target rates. Therefore, by adjusting target rates, we can achieve differences in performance analyses for BackCom NOMA-RIS and BackCom SR systems. The other performance curves are the same as the previous figures.

B. Impacts of RIS and NOMA to Outage Performance

If the RIS has a higher number of metasurface elements M, we need to examine how M affects the outage performance. As shown in Fig. 8, the higher M leads to the better outage probabilities for user D_2 . Especially at high SNR, it shows that the outage probabilities are very low. The reason is that

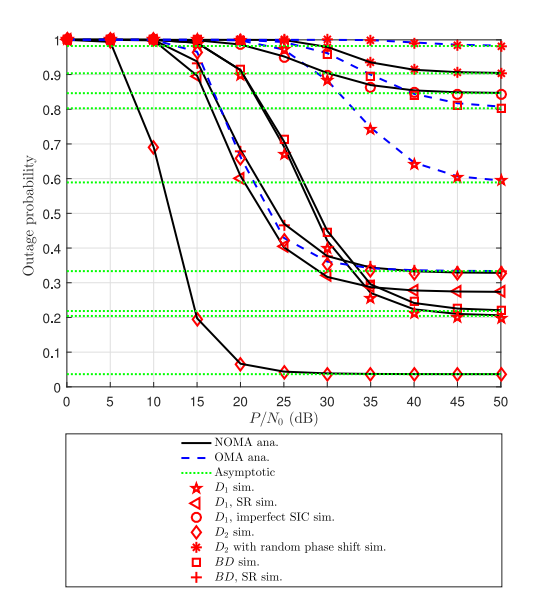


Fig. 9. Comparison of outage probability between BackCom NOMA-RIS with the benchmark (BackCom OMA-RIS).

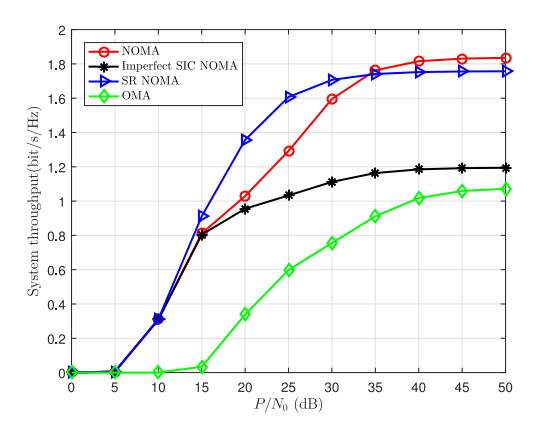


Fig. 10. Comparison of system throughput.

RIS intelligently varies its phases to maximize SINRs, then the better outage probability can be achieved. More importantly, by enabling the RIS, D_2 significantly outperforms D_1 , which confirms the benefit of deploying the RIS. The other performance curves can be similarly explained as the previous figures.

In Fig. 9, we compare the outage performance of BackCom NOMA-RIS with the counterparts, including both BackCom SR system [32] and BackCom OMA-RIS. It can be seen that user D_2 at BackCom NOMA-RIS with random phase shift shows its superiority compared with the two remaining systems. From this observation, the advances of RIS are firmly determined.

Fig. 10 depicts the throughput performance of BackCom NOMA-RIS which is determined as the highest one when the average SNR at BS is greater than 35 dB. The main reason is that throughput depends on outage probability which is indicated as smaller at the high SNR region. It can be intuitively seen that BackCom NOMA-RIS improves about 80% compared with the benchmark (BackCom OMA-RIS).

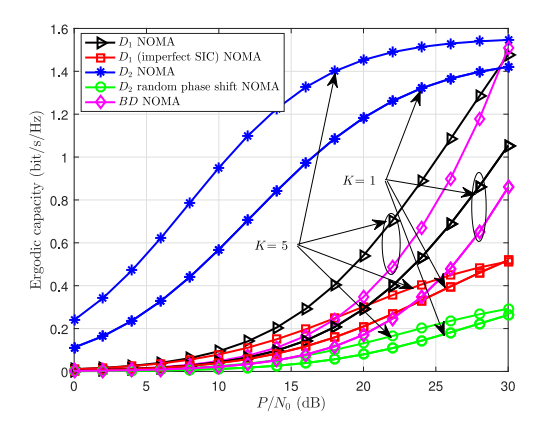


Fig. 11. Ergodic capacity versus P/N_0 as changing K.

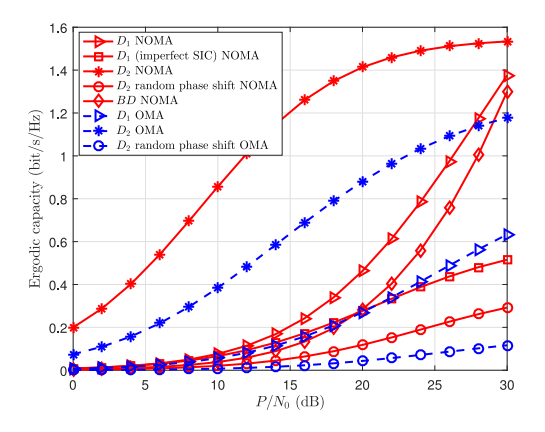


Fig. 12. Ergodic capacity versus P/N_0 : comparison between BackCom NOMA-RIS and BackCom OMA-RIS.

C. Impacts of TAS Scheme to Ergodic Capacity Performance

Fig. 11 demonstrates the ergodic capacity of two users in many considerations in terms of imperfect SIC and perfect SIC. At first look, it is shown that the ergodic capacity of the BackCom NOMA-RIS with more antennas at the BS (K=5) is always larger than that of the single antenna BackCom NOMA-RIS (K=1) and the capacity gap gradually narrows with the improvement of the channel conditions. This means that under the setting of antennas at the BS, the ergodic capacity can be improved significantly. Similarly, ergodic capacity in BackCom NOMA-RIS outperforms than benchmark (BackCom OMA-RIS), shown in Fig. 12.

VI. CONCLUSION

This article has analyzed the outage performance of a BackCom NOMA-RIS with two benchmark systems, i.e., BackCom SR system [32] and BackCom NOMA-RIS system, to highlight advances of backscatter, RIS, and NOMA techniques. In a two-user scenario, considering the downlink of an IoT system from the multiple antennas BS to users, each user can maximize its benefits, i.e., the cell-edge IoT device benefits from both RIS and the BD, while the cell-center IoT device only needs the help of the BD to remain its performance. We found closed-form expressions of the outage probabilities, and approximate closed-form expressions of the ergodic capacity to characterize the performance of each IoT device

in a considered cluster. We indicated that the outage probabilities and ergodic capacity can be adjusted by varying the main parameters, such as the number of antennas at the BS, power allocation factors, and target rates. Numerical results provided detailed comparisons along with explicit explanations to validate our analysis. The main finding is also confirmed that a higher metasurface designed at the RIS and more antennas equipped at the BS can improve the performance of the IoT devices significantly.

APPENDIX A PROOF OF PROPOSITION 1

It is noted that channels follow the Rayleigh distribution and their PDF and CDF of $X_{k^*} \in \{|h_{1k^*}|^2, |\widetilde{h}_{1k^*}|^2, Q_{1k^*}^2, Z_{k^*}^2, |v_{k^*}|^2\}$ can be written as

$$F_{X_{k^*}}(x) = 1 - \sum_{a=1}^{K} {K \choose a} (-1)^{a-1} e^{-\frac{ax}{\varphi_{X_{k^*}}}}$$
 (53)

$$f_{X_{k^*}}(x) = \sum_{a=1}^{K} {K \choose a} (-1)^{a-1} \frac{a}{\varphi_{X_1}} e^{-\frac{ax}{\varphi_{X_{k^*}}}}.$$
 (54)

The CDF and PDF of $Y \in \{|l_1|^2, |l_2|^2, |g_1|^2, |g_2|^2\}$ can be written as

$$F_Y(x) = 1 - e^{-\frac{x}{\varphi_Y}} \tag{55}$$

$$f_Y(x) = \frac{1}{\omega_Y} e^{-\frac{x}{\varphi_Y}}. (56)$$

From (8), Δ is given by

$$\Delta = \Pr\left(|h_{1k^*}|^2 \ge \frac{\gamma_{\text{th}2}(P\wp_1|v_{k^*}|^2|l_1|^2 + P_{d1}|g_1|^2 + N_0)}{(\beta_2 - \gamma_{\text{th}2}\beta_1)Pd_{h_1}^{-\partial}} \right.$$

$$|h_{1k^*}|^2 \ge \frac{\gamma_{\text{th}1}(P\wp_1|v_{k^*}|^2|l_1|^2 + P_{d1}|g_1|^2 + N_0)}{\beta_1Pd_{h_1}^{-\partial}}\right)$$

$$= \Pr\left(|h_{1k^*}|^2 \ge \Omega_1\left(P\wp_1|v_{k^*}|^2|l_1|^2 + P_{d1}|g_1|^2 + N_0\right)\right)$$

$$= \int_0^\infty \int_0^\infty \int_0^\infty \left\{1 - F_{|h_{1k^*}|^2}\left[\Omega_1(P\wp_1xy + P_{d1}z + N_0)\right]\right\}$$

$$\times f_{|v_{k^*}|^2}(x)f_{|l_1|^2}(y)f_{|g_1|^2}(z)dxdydz \tag{57}$$

where $\Omega_1=\max([\gamma_{\text{th}2}/((\beta_2-\gamma_{\text{th}2}\beta_1)Pd_{h_1}^{-\partial})],[\gamma_{\text{th}1}/(\beta_1Pd_{h_1}^{-\partial})])$. Based on (53), (54), and (56), then Δ can be calculated as

$$\Delta = \sum_{a=1}^{K} \sum_{b=1}^{K} {K \choose a} {K \choose b} (-1)^{a+b-2} \frac{be^{-\frac{a\Omega_{1}N_{0}}{\varphi_{1}}}}{\varphi_{\nu}\varphi_{l,1}\varphi_{g,1}}$$

$$\times \int_{0}^{\infty} e^{-\left(\frac{a\Omega_{1}P_{d1}}{\varphi_{1}} + \frac{1}{\varphi_{g,1}}\right)z} dz$$

$$\times \int_{0}^{\infty} \int_{0}^{\infty} e^{-\left(\frac{a\Omega_{1}P_{\varphi_{1}}y}{\varphi_{1}} + \frac{b}{\varphi_{\nu}}\right)x} e^{-\frac{y}{\varphi_{l,1}}} dxdy$$

$$= \sum_{a=1}^{K} \sum_{b=1}^{K} {K \choose a} {K \choose b} (-1)^{a+b-2} \frac{\varphi_{1}e^{-\frac{a\Omega_{1}N_{0}}{\varphi_{1}}}}{\varphi_{l,1}(a\Omega_{1}P_{d1}\varphi_{g,1} + \varphi_{1})}$$

$$\times \int_{0}^{\infty} \frac{b\varphi_{1}}{a\Omega_{1}P_{\varnothing_{1}}\varphi_{\nu}y + b\varphi_{1}} e^{-\frac{y}{\varphi_{l,1}}} dy. \tag{58}$$

Based on [33, eq. (3.352.4)] and applying some polynomial expansion manipulations, Δ is given by

$$\Delta = \sum_{a=1}^{K} \sum_{b=1}^{K} {K \choose a} {K \choose b} (-1)^{a+b-2} \frac{-\varphi_1 \chi_1}{a\Omega_1 P_{d1} \varphi_{g,1} + \varphi_1} \times e^{\chi_1 - \frac{a\Omega_1 N_0}{\varphi_1}} \text{Ei}(-\chi_1)$$
(59)

where $\chi_1 = (b\varphi_1/[a\Omega_1P\wp_1\varphi_\nu\varphi_{l,1}])$. Substituting (59) into (8), we can obtain (9). The proof is completed.

APPENDIX B PROOF OF PROPOSITION 2

From (10), Θ can be calculated as

$$\Theta = \Pr\left(\frac{\beta_{2}Pd_{h_{1}}^{-\partial}|h_{1k^{*}}|^{2}}{\beta_{1}Pd_{h_{1}}^{-\partial}|h_{1k^{*}}|^{2} + P_{\mathcal{O}1}|v_{k^{*}}|^{2}|l_{1}|^{2} + P_{d1}|g_{1}|^{2} + N_{0}}\right)$$

$$\geq \gamma_{\text{th}2}, \frac{\beta_{1}Pd_{h_{1}}^{-\partial}|h_{1k^{*}}|^{2}}{P_{\mathcal{O}1}|v_{k^{*}}|^{2}|l_{1}|^{2} + P_{d1}|g_{1}|^{2} + N_{0}}$$

$$\geq \gamma_{\text{th}1}, \frac{P_{\mathcal{O}1}|v_{k^{*}}|^{2}|l_{1}|^{2}}{P_{d1}|g_{1}|^{2} + N_{0}} \geq \gamma_{thb}$$

$$= \Pr\left(|h_{1k^{*}}|^{2} \geq \Omega_{1}\left(P_{\mathcal{O}1}|v_{k^{*}}|^{2}|l_{1}|^{2} + P_{d1}|g_{1}|^{2} + N_{0}\right)$$

$$|v_{k^{*}}|^{2}|l_{1}|^{2} \geq \frac{\gamma_{thb}}{P_{\mathcal{O}1}}\left(P_{d1}|g_{1}|^{2} + N_{0}\right)\right). \tag{60}$$

We assume $L = |v_{k^*}|^2 |l_1|^2$ with parameter $L \sim \exp(\varphi_v \varphi_{l,1})$ [32]. Then, Θ is given by

$$\begin{split} \Theta &= \int_{0}^{\infty} \int_{\frac{\gamma_{thb}}{P_{so_{1}}}(P_{d1}y+N_{0})}^{\infty} \\ &\times \left\{ 1 - F_{\left|h_{1k^{*}}\right|^{2}} \left[\Omega_{1}(P_{so_{1}x} + P_{d1}y + N_{0}) \right] \right\} \\ &\times f_{L}(x) f_{\left|g_{1}\right|^{2}}(y) dx dy \\ &= \sum_{a=1}^{K} \sum_{b=1}^{K} {K \choose a} {K \choose b} (-1)^{a+b-2} \frac{b}{\varphi_{v} \varphi_{l,1} \varphi_{g,1}} e^{-\frac{a\Omega_{1}N_{0}}{\varphi_{1}}} \\ &\times \int_{0}^{\infty} \int_{\frac{\gamma_{thb}}{P_{so_{1}}}(P_{d1}y+N_{0})}^{\infty} e^{-\chi_{2}x} e^{-\left(\frac{a\Omega_{1}P_{d1}}{\varphi_{1}} + \frac{1}{\varphi_{g,1}}\right)^{y}} dx dy \end{split}$$

$$= \sum_{a=1}^{K} \sum_{b=1}^{K} {K \choose a} {K \choose b} (-1)^{a+b-2} \frac{b\varphi_1}{\varphi_{g,1} \left(a\Omega_1 P \wp_1 \varphi_\nu \varphi_{l,1} + b\varphi_1\right)}$$

$$\times e^{-\frac{\chi_2 \gamma_{thb} N_0}{P_{\wp_1}} - \frac{a\Omega_1 N_0}{\varphi_1}} \int_0^\infty e^{-\chi_3 y} dy$$

$$= \sum_{a=1}^{K} \sum_{b=1}^{K} {K \choose a} {K \choose b} (-1)^{a+b-2} \frac{b\varphi_1}{\varphi_{g,1} \chi_3 \left(a\Omega_1 P \wp_1 \varphi_\nu \varphi_{l,1} + b\varphi_1\right)}$$

$$\times e^{-\frac{\chi_2 \gamma_{thb} N_0}{P_{\wp_1}} - \frac{a\Omega_1 N_0}{\varphi_1}}$$
(61)

where $\chi_2 = ([a\Omega_1 P \wp_1]/\varphi_1) + (b/[\varphi_\nu \varphi_{l,1}])$ and $\chi_3 = ([\chi_2 \gamma_{thb} P_{d1}]/P \wp_1) + ([a\Omega_1 P_{d1}]/\varphi_1) + (1/\varphi_{g,1})$. Substituting (61) into (10), we can obtain (11).

The proof is completed.

APPENDIX C PROOF OF PROPOSITION 3

From (13), $OP_{1,ip}$ is given as (62), shown at the bottom of the page.

In the following, we calculate $OP_{1,ip}$ in two cases.

Case I: Both $0 < \beta_1 < (\beta_2/\gamma_{\text{th}2}) \stackrel{\triangle}{=} u_2$ and we assume $\beta_2 P d_{h_1}^{-\partial} |\widetilde{h}_{1k^*}|^2 + P_{\wp_1}|v_{k^*}|^2 |l_1|^2 + P_{d1}|g_1|^2 + N_0 \approx P_{\wp_1}|v_{k^*}|^2 |l_1|^2 + P_{d1}|g_1|^2 + N_0$. Hence, we focus on the analysis for high SNR regime and adopt the following upper bounds $(\gamma_{\text{th}1}/[\beta_1 P d_{h_1}^{-\partial}]) > (\gamma_{\text{th}2}/[P d_{h_1}^{-\partial}(\beta_2 - \gamma_{\text{th}2}\beta_1)])$. This is equivalent to $0 < \beta_1 < ([\gamma_{\text{th}1}\beta_2]/[\gamma_{\text{th}2} + \gamma_{\text{th}1}\gamma_{\text{th}2}]) \stackrel{\triangle}{=} u_1$.

Case II: Both $0 < \beta_1 < u_2$ and $(\gamma_{\text{th}1}/[\beta_1 P d_{h_1}^{-\delta}]) < (\gamma_{\text{th}2}/[P d_{h_1}^{-\delta}(\beta_2 - \gamma_{\text{th}2}\beta_1)])$ hold. This is equivalent to $u_1 < \beta_1 < u_2$. Then, $OP_{1,ip}$ is given as shown in (63) at the bottom of the next page.

From (63), Z_1 is given as (64), shown at the bottom of the next page.

Based on [33, eq. (3.352.4)] and applying some polynomial expansion manipulations, Z_1 is given by

$$Z_{1} = -\sum_{a=1}^{K} \sum_{b=1}^{K} \sum_{c=1}^{K} {K \choose a} {K \choose b} {K \choose c} (-1)^{a+b+c-3}$$

$$\times \frac{b\beta_{1}\varphi_{1}}{a\gamma_{\text{th}1}\beta_{2}k_{1}\varphi_{ip} + b\beta_{1}\varphi_{1}} \frac{\beta_{1}Pd_{h_{1}}^{-\partial}\varphi_{1}\chi_{4}}{a\gamma_{\text{th}1}P_{d1}\varphi_{g,1} + \beta_{1}Pd_{h_{1}}^{-\partial}\varphi_{1}}$$

$$\times e^{\chi_{4} - \frac{a\gamma_{\text{th}1}N_{0}}{\beta_{1}Pd_{h_{1}}^{-\partial}\varphi_{1}}} \text{Ei}(-\chi_{4})$$
(65)

$$OP_{1,ip} = 1 - \Pr(\gamma_{1k^* \leftarrow 2} \ge \gamma_{\text{th}2}, \gamma_{1k^*,ip} \ge \gamma_{\text{th}1})$$

$$= 1 - \Pr\left(|h_{1k^*}|^2 \ge \frac{\gamma_{\text{th}2}}{Pd_{h_1}^{-\partial}(\beta_2 - \gamma_{\text{th}2}\beta_1)} \left(P\wp_1|v_{k^*}|^2|l_1|^2 + P_{d1}|g_1|^2 + N_0\right)\right)$$

$$|h_{1k^*}|^2 \ge \frac{\gamma_{\text{th}1}}{\beta_1 Pd_{h_1}^{-\partial}} \left(\beta_2 Pd_{h_1}^{-\partial}|\widetilde{h}_{1k^*}|^2 + P\wp_1|v_{k^*}|^2|l_1|^2 + P_{d1}|g_1|^2 + N_0\right)$$

$$= 1 - \Pr\left(|h_{1k^*}|^2 \ge \max\left(\frac{\gamma_{\text{th}1}}{\beta_1 Pd_{h_1}^{-\partial}} \left(\beta_2 Pd_{h_1}^{-\partial}|\widetilde{h}_{1k^*}|^2 + P\wp_1|v_{k^*}|^2|l_1|^2 + P_{d1}|g_1|^2 + N_0\right)\right)$$

$$\frac{\gamma_{\text{th}2}}{Pd_{h_1}^{-\partial}(\beta_2 - \gamma_{\text{th}2}\beta_1)} \left(P\wp_1|v_{k^*}|^2|l_1|^2 + P_{d1}|g_1|^2 + N_0\right)\right). \tag{62}$$

where $\chi_4 = ([c\beta_1 d_{h_1}^{-\partial} \varphi_1]/[a\gamma_{\text{th}1} \wp_1 \varphi_{\nu} \varphi_{l,1}])$. From (63), Z_2 is given as (66), shown at the bottom of the

Based on [33, eq. (3.352.4)] and applying some polynomial expansion manipulations, Z₂ is given by

$$Z_{2} = -\sum_{a=1}^{K} \sum_{b=1}^{K} {K \choose a} {K \choose b} (-1)^{a+b-2}$$

$$\times \frac{(\beta_{2} - \gamma_{\text{th}2}\beta_{1}) d_{h_{1}}^{-\partial} P \varphi_{1} \chi_{5}}{a \gamma_{\text{th}2} P_{d1} \varphi_{g,1} + (\beta_{2} - \gamma_{\text{th}2}\beta_{1}) d_{h_{1}}^{-\partial} P \varphi_{1}}$$

$$\times e^{\chi_{5} - \frac{a \gamma_{\text{th}2} N_{0}}{(\beta_{2} - \gamma_{\text{th}2}\beta_{1}) d_{h_{1}}^{-\partial} P \varphi_{1}}} Ei(-\chi_{5})$$

$$(67)$$

where $\chi_5 = ([(\beta_2 - \gamma_{\text{th}2}\beta_1)bd_{h_1}^{-\partial}\varphi_1]/[a\gamma_{\text{th}2}\wp_1\varphi_\nu\varphi_{l,1}]).$ Then, we can obtain (14).

The proof is completed.

APPENDIX D PROOF OF COROLLARY 1

By relying on (9), at high SNRs regime, the asymptotic expression for outage probability for D_1 with perfect SIC case is expressed by

$$OP_{1}^{\infty} = 1 + \sum_{a=1}^{K} \sum_{b=1}^{K} {K \choose a} {K \choose b} (-1)^{a+b-2} \times \frac{\frac{P}{N_{0}} \varphi_{1}}{a \Omega_{1}^{\infty} \frac{P_{d1}}{N_{0}} \varphi_{g,1} + \frac{P}{N_{0}} \varphi_{1}} \chi_{1}^{\infty} e^{\chi_{1}^{\infty}} e^{-\frac{a \Omega_{1}^{\infty} N_{0}}{P \varphi_{1}}} \operatorname{Ei}(-\chi_{1}^{\infty})$$
(68)

where $\Omega_1^{\infty} = \max([\gamma_{\text{th}2}/((\beta_2 - \gamma_{\text{th}2}\beta_1)d_{h_1}^{-\partial})], [\gamma_{\text{th}1}/(\beta_1d_{h_1}^{-\partial})]),$ $\chi_1^{\infty} = (b\varphi_1/[a\Omega_1^{\infty}\wp_1\varphi_v\varphi_{l,1}]).$ When $(P/N_0) \rightarrow \infty$, and $x \rightarrow \infty$ then $e^{-x} \rightarrow 1$, $([(P/N_0)\varphi_1]/[a\Omega_1^{\infty}(P_{d1}/N_0)\varphi_{g,1} + (P/N_0)\varphi_1]) \rightarrow 1$, and $-([a\Omega_1^{\infty}N_0]/P\varphi_1) \rightarrow 1$ and hence (25) can be obtained.

$$OP_{1,ip} = \begin{cases} 1 - \underbrace{\Pr\left(|h_{1k^*}|^2 \ge \frac{\gamma_{\text{th}1}}{\beta_1 P d_{h_1}^{-\partial}} \left(\beta_2 P d_{h_1}^{-\partial} |\widetilde{h}_{1k^*}|^2 + P\wp_1|v_{k^*}|^2 |l_1|^2 + P_{d1}|g_1|^2 + N_0\right)\right)}_{Z_1}, 0 < \beta_1 < u_1 \end{cases}$$

$$1 - \underbrace{\Pr\left(|h_{1k^*}|^2 \ge \frac{\gamma_{\text{th}2}}{P d_{h_1}^{-\partial} (\beta_2 - \gamma_{\text{th}2}\beta_1)} \left(P\wp_1|v_{k^*}|^2 |l_1|^2 + P_{d1}|g_1|^2 + N_0\right)\right)}_{Z_2}, u_1 < \beta_1 < u_2.$$

$$(63)$$

$$\begin{split} Z_{1} &= \Pr\left(|h_{1k^{*}}|^{2} \geq \frac{\gamma_{\text{th1}}\left(\beta_{2}Pd_{h_{1}}^{-\partial}|\widetilde{h}_{1k^{*}}|^{2} + P_{\mathcal{G}1}|v_{k^{*}}|^{2}|l_{1}|^{2} + P_{d1}|g_{1}|^{2} + N_{0}\right)}{\beta_{1}Pd_{h_{1}}^{-\partial}}\right) \\ &= \int_{0}^{\infty} \int_{0}^{\infty} \int_{0}^{\infty} \int_{0}^{\infty} \left(1 - F_{|h_{1k^{*}}|^{2}}\left(\frac{\gamma_{\text{th1}}\left(\beta_{2}Pd_{h_{1}}^{-\partial}x + P_{\mathcal{G}1}yz + P_{d1}t + N_{0}\right)}{\beta_{1}Pd_{h_{1}}^{-\partial}}\right)\right) f_{|\widetilde{h}_{1k^{*}}|^{2}}(x)f_{|v_{k^{*}}|^{2}}(y)f_{|l_{1}|^{2}}(z)f_{|g_{1}|^{2}}(t)dxdydzdt \\ &= \sum_{a=1}^{K} \sum_{b=1}^{K} \sum_{c=1}^{K} {K \choose a} {K \choose b} {K \choose b} {K \choose c} (-1)^{a+b+c-3} \frac{bc}{k_{1}\varphi_{ip}\varphi_{v}\varphi_{l,1}\varphi_{g,1}} e^{-\frac{\alpha\gamma_{\text{th1}}N_{0}}{\beta_{1}Pd_{h_{1}}^{-\partial}\varphi_{1}}} \int_{0}^{\infty} e^{-\left(\frac{\alpha\gamma_{\text{th1}}\beta_{2}z}{\beta_{1}\varphi_{1}} + \frac{b}{k_{1}\varphi_{ip}}\right)x} dx \\ &\times \int_{0}^{\infty} e^{-\left(\frac{\alpha\gamma_{\text{th1}}P_{d1}}{\beta_{1}Pd_{h_{1}}^{-\partial}\varphi_{1}} + \frac{1}{\varphi_{g,1}}\right)t} dt \int_{0}^{\infty} \int_{0}^{\infty} e^{-\left(\frac{\alpha\gamma_{\text{th1}}\beta_{1}z}{\beta_{1}d_{h_{1}}^{-\partial}\varphi_{1}} + \frac{c}{\varphi_{v}}\right)y} e^{-\frac{z}{\varphi_{l,1}}} dydz \\ &= \sum_{a=1}^{K} \sum_{b=1}^{K} \sum_{c=1}^{K} {K \choose a} {K \choose b} {K \choose c} (-1)^{a+b+c-3} \frac{b\beta_{1}\varphi_{1}}{\varphi_{l,1}(a\gamma_{\text{th1}}\beta_{2}k_{1}\varphi_{ip} + b\beta_{1}\varphi_{1})} \frac{\beta_{1}Pd_{h_{1}}^{-\partial}\varphi_{1}}{a\gamma_{\text{th1}}Pd_{1}\varphi_{g,1} + \beta_{1}Pd_{h_{1}}^{-\partial}\varphi_{1}} e^{-\frac{\alpha\gamma_{\text{th1}}N_{0}}{\beta_{1}Pd_{h_{1}}^{-\partial}\varphi_{1}}} \\ &\times \int_{0}^{\infty} \frac{c\beta_{1}d_{h_{1}}^{-\partial}\varphi_{1}}{a\gamma_{\text{th1}}\beta_{1}\varphi_{1}\varphi_{v,z} + c\beta_{1}d_{v}^{-\partial}\varphi_{1}} e^{-\frac{z}{\varphi_{l,1}}} dz. \end{cases} \tag{64}$$

$$Z_{2} = \Pr\left(|h_{1k^{*}}|^{2} \ge \frac{\gamma_{\text{th2}}(P_{\mathcal{O}1}|\nu_{k^{*}}|^{2}|l_{1}|^{2} + P_{d1}|g_{1}|^{2} + N_{0})}{(\beta_{2} - \gamma_{\text{th2}}\beta_{1})d_{h_{1}}^{-\partial}P}\right)$$

$$= \sum_{a=1}^{K} \sum_{b=1}^{K} {K \choose a} {K \choose a} {K \choose b} (-1)^{a+b-2} \frac{(\beta_{2} - \gamma_{\text{th2}}\beta_{1})d_{h_{1}}^{-\partial}P\varphi_{1}}{\varphi_{l,1}\left(a\gamma_{\text{th2}}P_{d1}\varphi_{g,1} + (\beta_{2} - \gamma_{\text{th2}}\beta_{1})d_{h_{1}}^{-\partial}P\varphi_{1}\right)} e^{-\frac{a\gamma_{\text{th2}}N_{0}}{(\beta_{2} - \gamma_{\text{th2}}\beta_{1})d_{h_{1}}^{-\partial}P\varphi_{1}}} \int_{0}^{\infty} \frac{(\beta_{2} - \gamma_{\text{th2}}\beta_{1})bd_{h_{1}}^{-\partial}\varphi_{1}}{a\gamma_{\text{th2}}\wp_{1}\varphi_{\nu}y + (\beta_{2} - \gamma_{\text{th2}}\beta_{1})bd_{h_{1}}^{-\partial}\varphi_{1}} e^{-\frac{y}{\varphi_{l,1}}} dy.$$
(66)

By relying on (14), at high SNRs regime, the asymptotic expression for outage probability for D_1 with perfect SIC in two cases.

Case I: When $0 < \beta_1 < u_1$, and $(P/N_0) \rightarrow \infty$, and $x \rightarrow \infty$ then $e^{-x} \rightarrow 1$, the asymptotic expression for outage probability for D_1 with perfect SIC is given by

$$OP_{1,ip}^{\infty} = 1 + \sum_{a=1}^{K} \sum_{b=1}^{K} \sum_{c=1}^{K} {K \choose a} {K \choose b} {K \choose c} (-1)^{a+b+c-3}$$

$$\times \frac{b\beta_1 \varphi_1 \chi_4}{a\gamma_{\text{th}1} \beta_2 k_1 \varphi_{ip} + b\beta_1 \varphi_1} \frac{\beta_1 \frac{P}{N_0} d_{h_1}^{-\partial} \varphi_1}{a\gamma_{\text{th}1} \frac{P_{d1}}{N_0} \varphi_{g,1} + \beta_1 \frac{P}{N_0} d_{h_1}^{-\partial} \varphi_1}$$

$$\times e^{\chi_4} e^{-\frac{a\gamma_{\text{th}1} N_0}{\beta_1 P d_{h_1}^{-\partial} \varphi_1}} \text{Ei}(-\chi_4)$$
(69)

where $([\beta_1(P/N_0)d_{h_1}^{-\partial}\varphi_1]/[a\gamma_{\text{th}1}(P_{d1}/N_0)\varphi_{g,1} + \beta_1(P/N_0)d_{h_1}^{-\partial}\varphi_1]) \to 1$, and $e^{-([a\gamma_{\text{th}1}N_0]/[\beta_1Pd_{h_1}^{-\partial}\varphi_1])} \to 1$. Therefore, we can obtain (26).

Case II: When $u_1 < \beta_1 < u_2$, and $(P/N_0) \rightarrow \infty$, and $x \rightarrow \infty$ then $e^{-x} \rightarrow 1$, the asymptotic expression for outage probability for D_1 with perfect SIC is given by

$$OP_{1,ip}^{\infty} = 1 + \sum_{a=1}^{K} \sum_{b=1}^{K} {K \choose a} {K \choose b} (-1)^{a+b-2}$$

$$\times \frac{(\beta_2 - \gamma_{\text{th}2}\beta_1) d_{h_1}^{-\partial} \frac{P}{N_0} \varphi_1}{a \gamma_{\text{th}2} \frac{P_{d1}}{N_0} \varphi_{g,1} + (\beta_2 - \gamma_{\text{th}2}\beta_1) d_{h_1}^{-\partial} \frac{P}{N_0} \varphi_1}$$

$$\times \chi_5 e^{\chi_5} e^{-\frac{a \gamma_{\text{th}2} N_0}{(\beta_2 - \gamma_{\text{th}2}\beta_1) d_{h_1}^{-\partial} P_{\varphi_1}}} \text{Ei}(-\chi_5)$$
(70)

where $([(\beta_2 - \gamma_{\text{th}2}\beta_1)d_{h_1}^{-\partial}[P/N_0]\varphi_1] / [a\gamma_{\text{th}2}[P_{d1}/N_0]\varphi_{g,1}] + (\beta_2 - \gamma_{\text{th}2}\beta_1)d_{h_1}^{-\partial}(P/N_0)\varphi_1]) \rightarrow 1$, and $e^{-([a\gamma_{\text{th}2}N_0]/[(\beta_2 - \gamma_{\text{th}2}\beta_1)d_{h_1}^{-\partial}P\varphi_1])} \rightarrow 1$. Therefore, we can obtain (26).

APPENDIX E PROOF OF COROLLARY 3

By considering (16) in case of $P/N_0 \to \infty$, and $x \to \infty$ then $e^{-x} \to 1$, the asymptotic expression for outage probability at D_2 in the high SNR region is given by

$$OP_{2}^{\infty} = 1 + \sum_{a=1}^{K} \sum_{b=1}^{K} {K \choose a} {K \choose b} (-1)^{a+b-2}$$

$$\times \frac{(\beta_{2} - \gamma_{\text{th}2}\beta_{1})\tau \frac{P}{N_{0}} M d_{sr}^{-\partial} d_{rd_{2}}^{-\partial}}{a\gamma_{\text{th}2} \frac{P_{d2}}{N_{0}} \varphi_{g,2} + (\beta_{2} - \gamma_{\text{th}2}\beta_{1})\tau \frac{P}{N_{0}} M d_{sr}^{-\partial} d_{rd_{2}}^{-\partial}}$$

$$\times \chi_{6} e^{\chi_{6}} e^{-\frac{a\gamma_{\text{th}2}N_{0}}{(\beta_{2} - \gamma_{\text{th}2}\beta_{1})\tau P M d_{sr}^{-\partial} d_{rd_{2}}^{-\partial}}}{e^{-\frac{\alpha\gamma_{\text{th}2}N_{0}}{(\beta_{2} - \gamma_{\text{th}2}\beta_{1})\tau P M d_{sr}^{-\partial} d_{rd_{2}}^{-\partial}}} \text{Ei}(-\chi_{6})$$
(71)

where $([(\beta_2 - \gamma_{\text{th}2}\beta_1)\tau(P/N_0)Md_{sr}^{-\partial}d_{rd_2}^{-\partial}]$ / $[a\gamma_{\text{th}2}(P_{d2}/N_0)\varphi_{g,2} + (\beta_2 - \gamma_{\text{th}2}\beta_1)\tau(P/N_0)Md_{sr}^{-\partial}d_{rd_2}^{-\partial}]) \rightarrow 1$, $e^{-([a\gamma_{\text{th}2}N_0]/[(\beta_2 - \gamma_{\text{th}2}\beta_1)\tau PMd_{sr}^{-\partial}d_{rd_2}^{-\partial}])} \rightarrow 1$.

We can rely on (24) for the case of RIS using random phase shift, and condition on $P/N_0 \to \infty$, and $x \to \infty$ then $e^{-x} \to 1$, the asymptotic expression of outage probability at D_2 in the

high SNR region is formulated by

$$OP_{2,r}^{\infty} = 1 + \sum_{a=1}^{K} \sum_{b=1}^{K} {K \choose a} {K \choose b} (-1)^{a+b-2}$$

$$\times \frac{(\beta_2 - \gamma_{\text{th}2}\beta_1)\tau \frac{P}{N_0} d_{sr}^{-\partial} d_{rd_2}^{-\partial} M \varphi_{sr} \varphi_{rd_2}}{a\gamma_{\text{th}2} \frac{P_{d2}}{N_0} \varphi_{g,2} + (\beta_2 - \gamma_{\text{th}2}\beta_1)\tau \frac{P}{N_0} d_{sr}^{-\partial} d_{rd_2}^{-\partial} M \varphi_{sr} \varphi_{rd_2}}$$

$$\times \chi_7 e^{\chi_7} e^{-\frac{a\gamma_{\text{th}2}N_0}{(\beta_2 - \gamma_{\text{th}2}\beta_1)\tau P d_{sr}^{-\partial} d_{rd_2}^{-\partial} M \varphi_{sr} \varphi_{rd_2}}} \text{Ei}(-\chi_7)$$
(72)

where $([(\beta_2 - \gamma_{th2}\beta_1)\tau(P/N_0)d_{sr}^{-\partial}d_{rd_2}^{-\partial}M\varphi_{sr}\varphi_{rd_2}]/[a\gamma_{th2}(P_{d2}/N_0)\varphi_{g,2} + (\beta_2 - \gamma_{th2}\beta_1)\tau(P/N_0)d_{sr}^{-\partial}d_{rd_2}^{-\partial}M\varphi_{sr}\varphi_{rd_2}]) \rightarrow 1,$ $e^{-([a\gamma_{th2}N_0]/[(\beta_2 - \gamma_{th2}\beta_1)\tau Pd_{sr}^{-\partial}d_{rd_2}^{-\partial}M\varphi_{sr}\varphi_{rd_2}])} \rightarrow 1.$

REFERENCES

- C. K. Singh and P. K. Upadhyay, "Overlay cognitive IoT-based fullduplex relaying NOMA systems with hardware imperfections," *IEEE Internet Things J.*, vol. 9, no. 9, pp. 6578–6596, May 2022.
- [2] M.-S. Van Nguyen, D.-T. Do, S. Al-Rubaye, S. Mumtaz, A. Al-Dulaimi, and O. A. Dobre, "Exploiting impacts of antenna selection and energy harvesting for massive network connectivity," *IEEE Trans. Commun.*, vol. 69, no. 11, pp. 7587–7602, Nov. 2021.
- [3] D.-T. Do, A.-T. Le, Y. Liu, and A. Jamalipour, "User grouping and energy harvesting in UAV-NOMA system with AF/DF relaying," *IEEE Trans. Veh. Technol.*, vol. 70, no. 11, pp. 11855–11868, Nov. 2021.
- [4] H. Liu, G. Li, X. Li, Y. Liu, G. Huang, and Z. Ding, "Effective capacity analysis of STAR-RIS-assisted NOMA networks," *IEEE Wireless Commun. Lett.*, vol. 11, no. 9, pp. 1930–1934, Sep. 2022.
- [5] X. Li, H. Liu, G. Li, Y. Liu, M. Zeng, and Z. Ding, "Effective capacity analysis of AmBC-NOMA communication systems," *IEEE Trans. Veh. Technol.*, vol. 71, no. 10, pp. 11257–11261, Oct. 2022.
- [6] L. Xu, W. Yin, X. Zhang, and Y. Yang, "Fairness-aware throughput maximization over cognitive heterogeneous NOMA networks for industrial cognitive IoT," *IEEE Trans. Commun.*, vol. 68, no. 8, pp. 4723–4733, Aug. 2020.
- [7] V. Chawla and D. S. Ha, "An overview of passive RFID," *IEEE Commun. Mag.*, vol. 45, no. 9, pp. 11–17, Sep. 2007.
- [8] D. Deng, X. Li, S. Dang, and K. Rabie, "Outage analysis for tag selection in reciprocal backscatter communication systems," vol. 11, no. 2, pp. 210–214, Feb. 2022.
- [9] M. Elsayed, A. Samir, A. A. A. El-Banna, X. Li, and B. M. ElHalawany, "When NOMA multiplexing meets symbiotic ambient backscatter communication: Outage analysis," *IEEE Trans. Veh. Technol.*, vol. 71, no. 1, pp. 1026–1031, Jan. 2022.
- [10] W. Ma, Z. Niu, W. Wang, S. He, and T. Jiang, "Covert communication with uninformed backscatters in hybrid active/passive wireless networks: Modeling and performance analysis," *IEEE Trans. Commun.*, vol. 70, no. 4, pp. 2622–2634, Apr. 2022.
- [11] X. Li et al., "Physical layer security of cognitive ambient backscatter communications for green Internet-of-Things," *IEEE Trans. Green Commun. Netw.*, vol. 5, no. 3, pp. 1066–1076, Sep. 2021.
- [12] S. Gong, X. Huang, J. Xu, W. Liu, P. Wang, and D. Niyato, "Backscatter relay communications powered by wireless energy beamforming," *IEEE Trans. Commun.*, vol. 66, no. 7, pp. 3187–3200, Jul. 2018.
- [13] Y. Ye, L. Shi, R. Q. Hu, and G. Lu, "Energy-efficient resource allocation for Wirelessly powered backscatter communications," *IEEE Commun. Lett.*, vol. 23, no. 8, pp. 1418–1422, Aug. 2019.
- [14] X. Li, Y. Zheng, M. Zeng, Y. Liu, and O. A. Dobre, "Enhancing secrecy performance for STAR-RIS NOMA networks," *IEEE Trans. Veh. Technol.*, vol. 72, no. 2, pp. 2684–2688, Feb. 2023.
- [15] W. U. Khan, J. Liu, F. Jameel, M. T. R. Khan, S. H. Ahmed, and R. Jäntti, "Secure backscatter communications in multi-cell NOMA networks: Enabling link security for massive IoT networks," in *Proc. IEEE Conf. Comput. Commun. Workshops (INFOCOM WKSHPS)*, 2020, pp. 213–218.
- [16] G. Yang, X. Xu, and Y.-C. Liang, "Resource allocation in NOMA-enhanced backscatter communication networks for wireless powered IoT," *IEEE Wireless Commun. Lett.*, vol. 9, no. 1, pp. 117–120, Jan. 2020.
- [17] J. Zhu, P. Gao, G. Chen, P. Xiao, and A. Quddus, "Index modulation for STAR-RIS assisted NOMA system," *IEEE Commun. Lett.*, vol. 27, no. 2, pp. 716–720, Feb. 2023.

- [18] K. Zhi, C. Pan, H. Ren, and K. Wang, "Statistical CSI-based design for reconfigurable intelligent surface-aided massive MIMO systems with direct links," *IEEE Wireless Commun. Lett.*, vol. 10, no. 5, pp. 1128–1132, May 2021.
- [19] Q. Gao, Y. Liu, X. Mu, M. Jia, D. Li, and L. Hanzo, "Joint location and beamforming design for STAR-RIS assisted NOMA systems," *IEEE Trans. Commun.*, vol. 71, no. 4, pp. 2532–2546, Apr. 2023.
- [20] S. Li, L. Bariah, S. Muhaidat, A. Wang, and J. Liang, "Outage analysis of NOMA-enabled backscatter communications with intelligent reflecting surfaces," *IEEE Internet Things J.*, vol. 9, no. 16, pp. 15390–15400, Aug. 2022.
- [21] Y. Zhuang, X. Li, H. Ji, and H. Zhang, "Exploiting intelligent reflecting surface for energy efficiency in ambient backscatter communicationenabled NOMA networks," *IEEE Trans. Green Commun. Netw.*, vol. 6, no. 1, pp. 163–174, Mar. 2022.
- [22] A. Hakimi, S. Zargari, C. Tellambura, and S. Herath, "IRS-enabled backscattering in a downlink non-orthogonal multiple access system," *IEEE Commun. Lett.*, vol. 26, no. 12, pp. 2984–2988, Dec. 2022.
- [23] H. Chen, G. Yang, and Y.-C. Liang, "Joint active and passive Beamforming for reconfigurable intelligent surface enhanced symbiotic radio system," *IEEE Wireless Commun. Lett.*, vol. 10, no. 5, pp. 1056–1060, May 2021.
- [24] J. Hu, Y.-C. Liang, and Y. Pei, "Reconfigurable intelligent surface enhanced multi-user MISO symbiotic radio system," *IEEE Trans. Commun.*, vol. 69, no. 4, pp. 2359–2371, Apr. 2021.
- [25] M. Elhattab, M. A. Arfaoui, C. Assi, and A. Ghrayeb, "RIS-assisted joint transmission in a two-cell downlink NOMA cellular system," *IEEE J. Sel. Areas Commun.*, vol. 40, no. 4, pp. 1270–1286, Apr. 2022.
- [26] M. Aldababsa, E. Güven, M. A. Durmaz, C. Göztepe, G. K. Kurt, and O. Kucur, "Unified performance analysis of antenna selection schemes for cooperative MIMO-NOMA with practical impairments," *IEEE Trans. Wireless Commun.*, vol. 21, no. 6, pp. 4364–4378, Jun. 2022.
- [27] J. Zuo, Y. Liu, L. Yang, L. Song, and Y.-C. Liang, "Reconfigurable intelligent surface enhanced NOMA assisted backscatter communication system," *IEEE Trans. Veh. Technol.*, vol. 70, no. 7, pp. 7261–7266, Jul. 2021.
- [28] Q. Zhang, Y.-C. Liang, and H. V. Poor, "Reconfigurable intelligent surface assisted MIMO symbiotic radio networks," *IEEE Trans. Commun.*, vol. 69, no. 7, pp. 4832–4846, Jul. 2021.
- [29] M. Wu, X. Lei, X. Zhou, Y. Xiao, X. Tang, and R. Q. Hu, "Reconfigurable intelligent surface assisted spatial modulation for symbiotic radio," *IEEE Trans. Veh. Technol.*, vol. 70, no. 12, pp. 12918–12931, Dec. 2021.
- [30] J. Hu, Y. Pei, Y.-C. Liang, and S. Sun, "Reconfigurable intelligent surface based uplink massive MIMO symbiotic radio system," in *Proc. IEEE Global Commun. Conf. (GLOBECOM)*, 2021, pp. 1–6.
- [31] A. Bhowal, S. Aïssa, and R. S. Kshetrimayum, "RIS-assisted advanced spatial modulation techniques for ambient backscattering communications," *IEEE Trans. Green Commun. Netw.*, vol. 5, no. 4, pp. 1684–1696, Dec. 2021.
- [32] Q. Zhang, L. Zhang, Y.-C. Liang, and P.-Y. Kam, "Backscatter-NOMA: A symbiotic system of cellular and Internet-of-Things networks," *IEEE Access*, vol. 7, pp. 20000–20013, 2019.
- [33] I. S. Gradshteyn and I. M. Ryzhik, Table of Integrals, Series and Products. New York, NY, USA: Academic Press, 2000.
- [34] G. R. MacCartney and T. S. Rappaport, "Millimeter-wave base station diversity for 5G coordinated multipoint (CoMP) applications," *IEEE Trans. Wireless Commun.*, vol. 18, no. 7, pp. 3395–3410, Jul. 2019.
- [35] X. Li et al., "Hardware impaired ambient backscatter NOMA systems: Reliability and security," *IEEE Trans. Commun.*, vol. 69, no. 4, pp. 2723–2736, Apr. 2021.
- [36] X. Xie, F. Fang, and Z. Ding, "Joint optimization of beamforming, phase-shifting and power allocation in a multi-cluster IRS-NOMA network," *IEEE Trans. Veh. Technol.*, vol. 70, no. 8, pp. 7705–7717, Aug. 2021.
- [37] P. Yang, L. Yang, W. Kuang, and S. Wang, "Outage performance of cognitive radio networks with a coverage-limited RIS for interference elimination," *IEEE Wireless Commun. Lett.*, vol. 11, no. 8, pp. 1694–1698, Aug. 2022.
- [38] W. Zhao, G. Wang, S. Atapattu, T. A. Tsiftsis, and C. Tellambura, "Is backscatter link stronger than direct link in reconfigurable intelligent surface-assisted system?" *IEEE Commun. Lett.*, vol. 24, no. 6, pp. 1342–1346, Jun. 2020.
- [39] H. Ma, H. Zhang, N. Zhang, J. Wang, N. Wang, and V. C. M. Leung, "Reconfigurable intelligent surface with energy harvesting assisted cooperative ambient backscatter communications," *IEEE Wireless Commun. Lett.*, vol. 11, no. 6, pp. 1283–1287, Jun. 2022.

- [40] Z. Abdullah, G. Chen, S. Lambotharan, and J. A. Chambers, "A hybrid relay and intelligent reflecting surface network and its Ergodic performance analysis," *IEEE Wireless Commun. Lett.*, vol. 9, no. 10, pp. 1653–1657, Oct. 2020.
- [41] J. He, K. Yu, Y. Shi, Y. Zhou, W. Chen, and K. B. Letaief, "Reconfigurable intelligent surface assisted massive MIMO with antenna selection," *IEEE Trans. Wireless Commun.*, vol. 21, no. 7, pp. 4769–4783, Jul. 2022.
- [42] W. U. Khan, A. Ihsan, T. N. Nguyen, Z. Ali, and M. A. Javed, "NOMA-enabled backscatter communications for green transportation in automotive-industry 5.0," *IEEE Trans. Ind. Informat.*, vol. 18, no. 11, pp. 7862–7874, Nov. 2022.
- [43] H. Wang, Z. Shi, Y. Fu, and S. Fu, "On intelligent reflecting surface-assisted NOMA Uplinks with imperfect SIC," *IEEE Wireless Commun. Lett.*, vol. 11, no. 7, pp. 1518–1522, Jul. 2022.
- [44] T. Van Chien, L. T. Tu, S. Chatzinotas, and B. Ottersten, "Coverage probability and Ergodic capacity of intelligent reflecting surface-enhanced communication systems," *IEEE Commun. Lett.*, vol. 25, no. 1, pp. 69–73, Jan. 2021
- [45] Q. Wu and R. Zhang, "Intelligent reflecting surface enhanced wireless network via joint active and passive beamforming," *IEEE Trans. Wireless Commun.*, vol. 18, no. 11, pp. 5394–5409, Nov. 2019.
- [46] E. Bjornson, O. Ozdogan, and E. G. Larsson, "Intelligent reflecting surface versus decode-and-forward: How large surfaces are needed to beat relaying?" *IEEE Wireless Commun. Lett.*, vol. 9, no. 2, pp. 244–248, Feb. 2020.



Minh-Sang Van Nguyen was born in Ben Tre, Vietnam. He is currently pursuing the master's degree in computer science with Ton Duc Thang University, Ho Chi Minh City, Vietnam.

He worked with the Industrial University of Ho Chi Minh City, Ho Chi Minh City, from 2018 to 2022. He has authored or coauthored over 22 peer-reviewed journals (SCIE), one book chapter and one conference paper. His research interests include electronic design, signal processing in wireless communications networks, nonorthogonal multiple access,

reconfigurable intelligent surfaces, and physical-layer security.

Mr. Nguyen was a reviewer of WCNC conferences, IEEE ACCESS, International Journal of Electronics, and Eurasip Journal on Wireless Communications and Networking.



Dinh-Thuan Do (Senior Member, IEEE) received the B.S., M.Eng., and Ph.D. degrees in communications engineering from Vietnam National University-Ho Chi Minh City, Ho Chi Minh City, Vietnam, in 2003, 2007, and 2013, respectively.

Before joining the University of Mount Union, Alliance, OH, USA, he was with the University of Colorado at Denver, Denver, CO, USA, as a Postdoctoral Fellow in 2022. He also worked as a Research Scientist with The University of Texas at Austin, Austin, TX, USA, in 2021 and as an

Assistant Professor with Asia University, Taichung, Taiwan, from 2020 to 2021. He published one textbook and five edited books. He has authored or coauthored over 100 technical papers published in peer-reviewed international journals (SCIE). His research interest includes signal processing in wireless communications network, reconfigurable intelligent surfaces, nonorthogonal multiple access network, satellite system, physical-layer security, device-to-device transmission, and energy harvesting.

Dr. Do was a recipient of the Golden Globe Award from the Vietnam Ministry of Science and Technology in 2015 (top 10 talented young scientists nationwide). He got the Creative Young Medal in 2015. He was named to the top list of 14 Highly Cited Scientists at Asia University in 2021. He was rewarded as the Best Editor of *ICT Express* in July 2023. He is serving as an Associate Editor for IEEE Transactions on Vehicular Technology and *Computer Communications*.



Alireza Vahid (Senior Member, IEEE) received the B.Sc. degree in electrical engineering from Sharif University of Technology, Tehran, Iran, in 2009, and the M.Sc. and Ph.D. degrees in electrical and computer engineering from Cornell University, Ithaca, NY, USA, in 2012 and 2015, respectively.

From 2015 to 2017, he worked as a Postdoctoral Research Scientist with the Information Initiative, Duke University, Durham, NC, USA, and from 2017 to 2023, he was an Assistant Professor of Electrical Engineering with University of Colorado at Denver,

Denver, CO, USA. He is currently a Gleason Chair Associate Professor of Electrical and Microelectronic Engineering with Rochester Institute of Technology, Rochester, NY, USA. His research interests include network information theory, wireless communications, and data storage.

Dr. Vahid received the 2015 Outstanding Ph.D. Thesis Research Award from Cornell University, the Qualcomm Innovation Fellowship in 2013, the Lab Venture Challenge Award in 2019, and the SONY Faculty Innovation Award in 2021. He currently serves as an Associate Editor for IEEE COMMUNICATIONS LETTERS.



Sami Muhaidat (Senior Member, IEEE) received the Ph.D. degree in electrical and computer engineering from the University of Waterloo, Waterloo, ON, Canada, in 2006.

From 2007 to 2008, he was an NSERC Postdoctoral Fellow with the Department of Electrical and Computer Engineering, University of Toronto, Toronto, ON, Canada. From 2008 to 2012, he was an Assistant Professor with the School of Engineering Science, Simon Fraser University, Burnaby, BC, Canada. He is currently a Professor

with Khalifa University, Abu Dhabi, UAE, and an Adjunct Professor with Carleton University, Ottawa, ON, Canada. His research interests focus on advanced digital signal processing techniques for wireless communications, intelligent surfaces, MIMO, optical communications, massive multiple access techniques, backscatter communications, and machine learning for communications.

Prof. Muhaidat is currently an Area Editor of the IEEE TRANSACTIONS ON COMMUNICATIONS, a Guest Editor of the IEEE NETWORK "Native Artificial Intelligence in Integrated Terrestrial and Nonterrestrial Networks in 6G" Special Issue, and a Guest Editor of the IEEE OPEN JOURNAL OF VEHICULAR TECHNOLOGY "Recent Advances in Security and Privacy for 6G Networks" Special Issue. He served as a Senior Editor and an Editor for the IEEE COMMUNICATIONS LETTERS, an Editor for the IEEE TRANSACTIONS ON COMMUNICATIONS, and an Associate Editor for the IEEE TRANSACTIONS ON VEHICULAR TECHNOLOGY.



Douglas Sicker (Senior Member, IEEE) received the B.S., M.S., and Ph.D. degrees in telecommunications from the University of Pittsburgh, Pittsburgh, PA, USA, in 1989, 1992, and 2001, respectively.

He is the Vice Chancellor of Technology and the CTO as well as a Professor of Computer Science and Electrical Engineering with the University of Colorado at Denver, Denver, CO, USA, and the University of Colorado at Anschutz, Aurora, CO, USA. He is also the Executive Director of

Broadband Internet Technical Advisory Group and the Co-Director of the Institute for Regulatory Law and Economics. Previously, he served as the Lord Endowed Chair of Engineering, the Department Head, an Interim Director of CyLab, and a Professor of Computer Science with Carnegie Mellon University, Pittsburgh. Previously, he was the DBC Endowed Professor with the Department of Computer Science, University of Colorado at Boulder, Boulder, CO, USA, with a joint appointment in, and the Director of, the Interdisciplinary Telecommunications Program. He served as the Chief Technology Officer and a Senior Advisor of Spectrum with the National Telecommunications and Information Administration, Washington, DC, USA. He also served as the CTO of the Federal Communications Commission (FCC) and prior to this, he served as a Senior Advisor on the FCC National Broadband Plan. Earlier, he was the Director of Global Architecture at Level 3 Communications, Inc. In the late 1990s, he served as the Chief of the Network Technology Division, FCC. He publishes and teaches in the fields of wireless systems, cybersecurity, and network policy.